Award Accounts

The Chemical Society of Japan Award for Creative Work for 2009

Hybridized Organic Nanocrystals for Optically Functional Materials

Hidetoshi Oikawa

Institute of Multidisciplinary Research for Advanced Materials (IMRAM), Tohoku University, 2-1-1 Katahira, Aoba-ku, Sendai 980-8577

Received August 4, 2010; E-mail: oikawah@tagen.tohoku.ac.jp

Organic nanocrystals (NCs) are in the mesoscopic phase between a single molecule and the corresponding bulk crystals, and are expected to exhibit peculiar optical properties, depending on crystal size and shape. In the present Award Accounts, recent progress on hybridized organic NCs and ordered array structure of encapsulated organic NCs will be introduced in detail for optically functional materials toward next-generation organic device application. Hybrid material (or hybridization) is an important area in current material science. Our attention is now focused on core–shell type hybridized organic NCs, which seem to be the best suited nanostructure for providing novel optoelectronic properties and photonic function induced by core–shell interface interaction. On the other hand, it may be necessary to arrange and integrate organic NCs, including hybridized materials, on a substrate so as to receive and transmit input and output signals by electronically and/or optically accessing organic devices. Hence, encapsulations of organic NCs, patterned substrates, and tapered cell method have been employed suitably to fabricate and control ordered array structure of organic NCs on a substrate. Finally, the future scope in the relevant fields of optoelectronics and photonics will be discussed in brief.

1. Introduction

"Hybrid and hybridization" is one of the most important and interesting topics in current material science and technology.[1–5] The original meaning of hybrid is the offspring of two different species or varieties of animals or plants. This definition should let us recall remarkably a different inner structure and novel physical properties that would be different from original material components. Hybridized materials are roughly divided into three categories:[1–5] (1) inorganic–inorganic systems such as metal alloys and semiconductor–metal systems, (2) organic–organic combinations like polymer blends and polymer alloys,[6] and (3) organic–inorganic (metal, semiconductor, ceramics, carbon material, and so on) hybridized materials,[1–5] e.g., polymer composites, organic silica, etc. For example, polymer blends and polymer composites are commonly produced by the following techniques:[6] dissolution using a cosolvent, mechanical mixing in a dry state, sol–gel reaction in a polymer matrix, and in situ polymerization in the presence of previously surface-modified inorganic fillers. As a result, hybridized polymer materials could exhibit useful properties and excellent functions in industrial products, which would ordinarily exhibit an additive and/or intermediate features between the original material components.

The domain size in these hybridized materials is usually on more or less a micrometer scale, and now great effort is being expended to reduce this to a nanometer scale for further improving application potential such as polymer nanocomposites,[6] in which nanometer-sized inorganic fillers are loaded and randomly dispersed in a matrix. Similarly, grain size is often controlled as possibly on a nanometer scale even in bulk metal alloy in order to bring out desired metal properties. In any case, the interface interaction between domains or between a domain and the surrounding material matrix is the most definitive and dominant factor determining properties and functions in hybridized materials.[1–6] Hence, intermediate states, quasi-static stable structures, and dynamic structure including relaxation process at the interface have been extensively investigated so far, and this research is a still main theme in the fields of catalyst, semiconductors, metal alloys, electrode materials, material composites, and artificial bio-related materials. In particular, hetero nanointerfaces in polymer nanocomposites are much attractive for creating novel hybridized materials.[6] However, the size of these hybridized materials is still above micrometer scale, and the material matrix itself is usually in a bulk state.

On the other hand, hybridized nanomaterials, the overall size of which is already on a nanometer scale, should be essentially distinguished from the above-mentioned hybridized materials, and have attracted great attention in nanoscience.[7–15] The components in hybridized nanomaterials are commonly metal nanoparticles (NPs),[16–18] and semiconductor NPs (or semiconductor quantum dots: SQDs),[19–21] magnetic NPs,[22] and π-conjugated organic and polymer nanocrystals (hereinafter, called organic NCs) and/or NPs,[23–25] and their physical properties are of much interest, e.g., localized surface plasmon

Published on the web February 26, 2011; doi:10.1246/bcsj.20100215

(LSP),[16–18] quantum confinement effects,[19–21] giant magneto resistive effects,[22] and optoelectronic size effect.[23–25] In particular, hybridized core–shell type nanomaterials are expected to exhibit peculiar properties, resulting from mutual interactions coupled between excitons (or delocalized electronic state) from a π-conjugated component and LSP from a noble metal component at the core–shell hetero nanointerface (hereinafter, called "core–shell interface"),[13,14,26–31] which are strongly dependent on overall size (or total volume), core–shell volume ratio (core radius and shell thickness), and the combination of core–shell original material components.[10–12] Conversely it is said that core–shell type hybridized nanomaterials may be the most suitable nanostructure for producing notable optoelectronic, photonic, redox, conductive, and catalytic functions, which would be affected remarkably by thermally metastable nanostructure, electronic state and exciton, LSP, optical response, etc. at the core–shell interface.[32] However, mutual interaction at the core–shell interface has not been necessarily investigated in the same way as interaction at the hetero nanointerface in hybridized materials,[33] although heterojunctions have been studied extensively so far in semiconductors. In other words, it should be necessary to highly control and construct well-defined core–shell nanostructure to precisely understand this kind of mutual interaction at the core–shell interface.[32]

Noble metal NPs, semiconductor NPs, and SQDs, as a component in core–shell type hybridized nanomaterials, have been so far and continue to be still now researched extensively,[16–21] compared with organic NCs.[23–25] As is known, Prof. T. Hayashi started the JST Project "Super Fine Particles" in the 1980s. On the other hand, polymer colloids and microspheres have been already established as industrial materials. On the contrary, research with regard to organic NCs have begun in earnest in 1992 by developing the preparation processes of reprecipitation method.[34]

π-Conjugated organic NCs are in an intermediate state between a single molecule and the corresponding bulk crystal.[23–25] The crystal size is usually in the range of several tens of nanometers to submicrometer, which can be controlled conveniently by optimizing the used good and poor solvents, the concentration and amount of the injected solution, temperature and stirring rate of poor solvent, added surfactant, and so on in the reprecipitation conditions.[35–42] These kinds of organic NCs are also expected to provide new size-dependent physical properties and peculiar optoelectronic and photonic function.[23–25,43–52] In fact, the following materials have been successfully nanocrystallized:[23–25,53–62] polydiacetylene (PDA), low-molecular-weight aromatic compounds like perylene and C_{60}, photochromic compounds of diarylethene, organic and ionic functional chromophores such as pseudo-isocyanine, merocyanine, phthalocyanine, and DAST (4′-dimethylamino-*N*-methylstilbazolium *p*-toluenesulfonate). PDA is one of the most promising organic nonlinear optical (NLO) materials,[63] which means large third-order NLO susceptibility $\chi^{(3)}(\omega)$ with very fast optical response.[64–66] Organic NCs have been also investigated in detail after developing the reprecipitation methods: i.e., nanocrystallization processes to further control crystal size and shape[42,67,68] the size dependence of linear optical properties and reactivity in solid-state polymerization,[23,49,50,52,69] the enhanced NLO properties in layered thin films of PDA NCs prepared by layer-by-layer technique,[23,70–72] and applied electric- or magnetic-field-induced orientation of "liquid and crystal" systems consisting of DAST NCs dispersion liquids.[51,73–75]

It goes without saying that more creative research fields concerning highly optical functional organic NCs, that is to say, "*New Creation of Hybridized Organic NCs*,"[76–85] should be advanced intensively toward next-generation organic optoelectronic and photonic device applications. Hence, the following three strategic research items have been made a plan for achieving this objective: (1) mass production of organic NCs for hybridization and encapsulation by introducing pulseless syringe pumps and microwave irradiation process into conventional reprecipitation method, (2) development of fabrication methods to produce core–shell type hybridized nanomaterials such as hybridized organic NCs, e.g., "visible-light-driven photocatalytic reduction method" (hereinafter, called "photocatalytic reduction method")[85] and "co-reprecipitation method,"[77] and (3) ordered array structures of organic and/or hybridized organic NCs on a substrate for device applications by using an encapsulation technique, lithographically patterned substrates and tapered cell method.[86–93] These above-mentioned three research items will be described and discussed in detail in the present Award Accounts.

2. Mass Production of Organic Nanocrystals

As described in the Introduction, organic NCs are commonly prepared by conventional reprecipitation method,[34] in which the crystal size and shape can be basically controlled by optimizing reprecipitation conditions: the combination of good and poor solvents, the amount and concentration of the injected solution, the injection rate and pressure, the temperature and stirring speed of poor solvent, and the addition of surfactants.[23–25,34] Under the typical reprecipitation conditions, a target compound is first dissolved in a water-miscible organic solvent such as alcohol, acetone, or THF. The concentration is usually on the order of mM, and a few hundred microliters of this diluted solution are quickly injected into vigorously stirred water (10 mL) as a poor solvent at a given temperature using a microsyringe. The target compound is immediately reprecipitated and then nanocrystallized in an aqueous medium. Namely, one can prepare successfully an aqueous dispersion liquid of organic NCs, which looks like an ordinary solution with low scattering loss, because the crystal size is normally below the wavelength of vis light region. Most organic NCs exhibit highly negative surface potential (ζ-potential),[23–25] and are dispersed stably in water medium for a long period, i.e., more than a few months to half a year. In the case of PDA, diacetylene (DA) monomer NCs are first obtained by the reprecipitation method,[23] and then further solid-state polymerized in an aqueous dispersion liquid by UV-irradiation ($\lambda =$ 254 nm) to convert DA monomer NCs into PDA NCs.[94–96] Conventional reprecipitation method has been improved so far, depending on the chemistry of target compounds. For example, supercritical reprecipitation method is effective in the case of phthalocyanine derivatives,[54,55] which are slightly insoluble in common organic solvents at room temperature. On the other hand, the inverse-reprecipitation method is applicable for

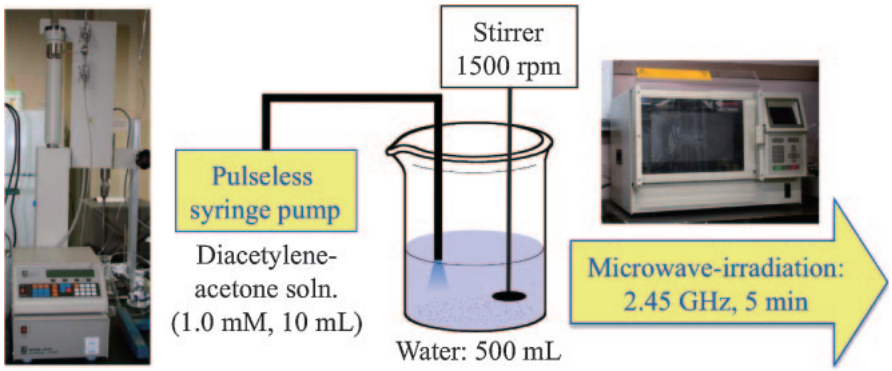

Figure 1. Scheme of the improved reprecipitation method for mass production and size-distribution control by introducing pulseless syringe pump and microwave irradiation process.

water-soluble organic and ionic functional chromophores as mentioned in the Introduction.[73–75] Good solvent is typically ethanol, while *n*-hexane and decalin are used as a poor medium in this case.

There are basically the two problems with these reprecipitation methods. One is mass production, and the other is the size-distribution control. These are closely related to characterization and application of organic NCs as described later. Pulseless syringe pumps[58] (Teledyne, 260D, Japan) and microwave irradiation process[56,57,59,60] (Perkin-Elmer, MULTIWAVE, USA) were introduced to conventional reprecipitation process in order to overcome the above-mentioned problems as schematically demonstrated in Figure 1. Namely, ca. 10 mL of target compound solution is continuously injected into 500 mL of water (stirring speed: 1500 rpm) at the injection rate of 10 mL min^{-1} with a pulseless syringe pump, instead of by microsyringe used in conventional reprecipitation method. Just after injection, the organic NCs dispersion liquid is immediately heated with microwave irradiation (2.45 GHz, 5 min), and then cooled to room temperature. As a result, for example, the obtained amount of PDA NCs per unit operation was of the order of mg and about one hundred fold improvement of these reprecipitation conditions for mass production. In addition, Figure 2 indicates the size distribution of PDA NCs evaluated by dynamic light scattering (DLS) (Otsuka Electronics, DLS-7000, Japan) measurement. Compared with the previous results (Figure 2a), the size distribution is considerably narrow in the improved reprecipitation method as shown in Figure 2b, and the standard deviation in the size distribution decreased considerably by an order of magnitude. The scanning electron microscopy (SEM) (JEOL, JSM-6700F, Japan) image (inset in Figure 2b) indicates almost monodisperse PDA NCs. Probably, the injection conditions, that is, injection rate and stirring speed of poor solvent, in the improved reprecipitation method provided a higher degree of supersaturation and reduced some experimental errors, e.g., aggregation phenomena on the wall of the glass vessel in the case of small scale of the conventional reprecipitation method.[23–25] In general, higher supersaturation would effectively promote more homogenous nucleation and crystal growth of PDA NCs,[42,67,68] efficiently producing monodisperse PDA NCs could be produced efficiently on a massive scale.

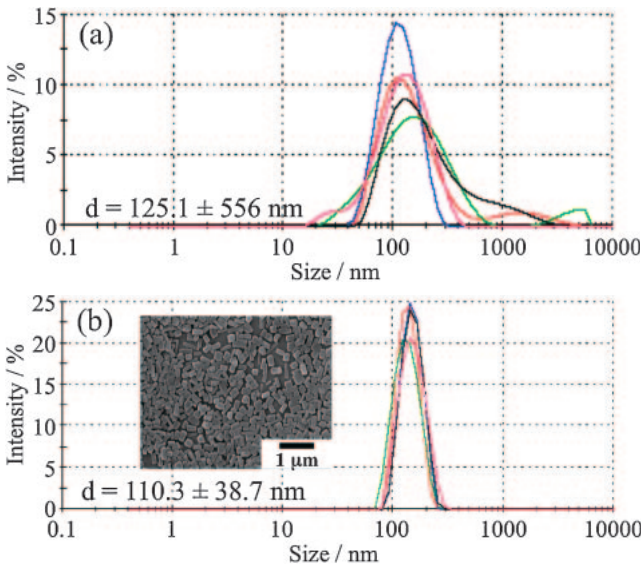

Figure 2. Size distribution of PDA NCs evaluated by DLS measurement: (a) conventional and (b) improved reprecipitation methods (Inset: SEM image of PDA NCs). The size-distribution curves with different colors demonstrate the data for every experiment, i.e., reproducibility, in both (a) and (b).

Successful mass production and narrow size distribution in PDA NCs are very important to make a possible of hybridization and encapsulation as described later.

3. Size Dependence of Linear Optical Properties in Organic Nanocrystals

Figure 3 demonstrates the typical extinction spectrum (JEOL, V-570, Japan) of PDA NCs dispersed in an aqueous medium.[23–25] The excitonic absorption peak (EAP) positions, λ_{max}, were clearly blue-shifted with decreasing crystal size. This behavior is similar to the quantum confinement effect in semiconductor NPs and SQD of single nanometer size.[19–21] The crystal size of organic NCs, however, is approximately ten to fifty times that of an ordinary SQD, and this size dependence is likely to be a phenomenon proper to organic NCs. On the other hand, the size dependence was also observed in the fluorescence emission spectrum in perylene NCs.[23–25,40] Put simply,

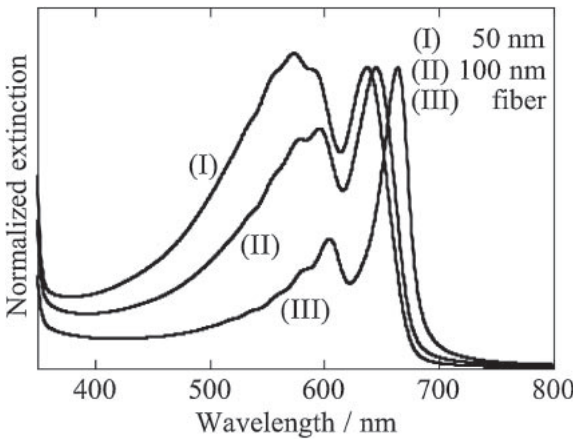

Figure 3. Extinction spectral changes of PDA NCs with decreasing crystal size in an aqueous dispersion medium.

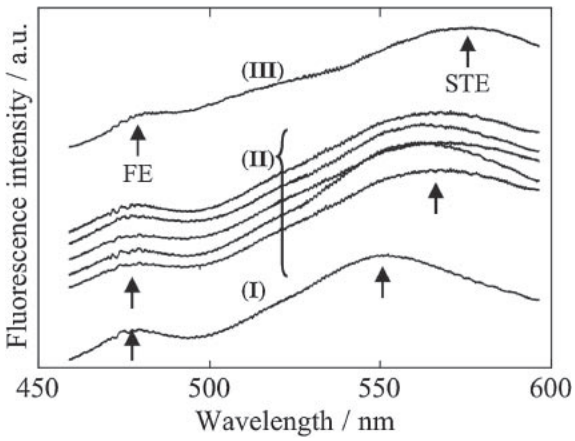

Figure 5. Fluorescence emission spectra for a single perylene NC with different crystal size: (I) 394, (II) 545, and (III) 634 nm.

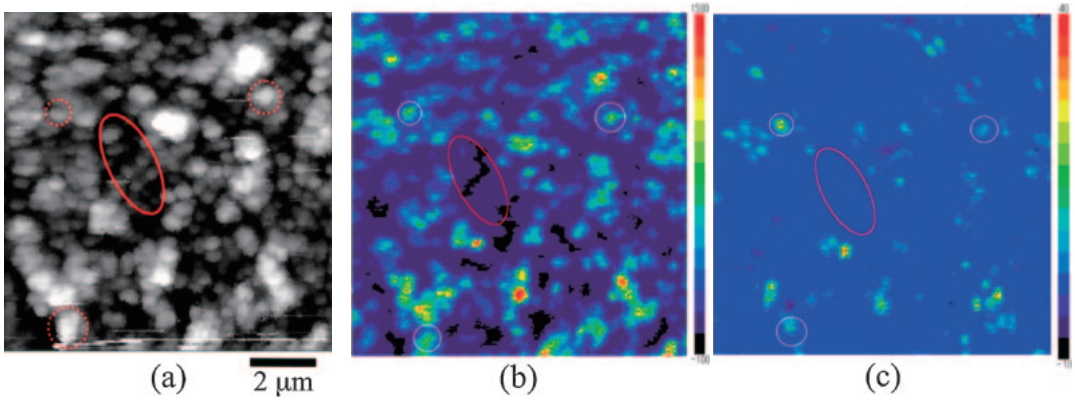

Figure 4. Topography and the corresponding fluorescence images of perylene NCs by the measurement with SNOM: (a) topography, (b) the corresponding fluorescence intensity image (wavelength range: 520 to 600 nm), and (c) the same image (wavelength range: 450 to 520 nm).

the fluorescence emission peak positions, λ_{max}, from self-trapped exciton (STE) levels were blue-shifted, when the crystal size was reduced continuously. However, these size dependences of linear optical properties are ensemble-averaged data in organic NCs dispersion systems, even though the size distribution narrows considerably as mentioned in Section **2**. Therefore, one has to investigate the relationship between linear optical properties and crystal size in an individual organic NC by measurement with scanning near-field optical microspectroscopy (SNOM) so as to clarify the mechanism of size dependence and shifts of λ_{max} on spectra.[49] SNOM enabled us to provide simultaneously the crystal size and spectral data in a single organic NC.

Figure 4 exhibits the topography and the corresponding fluorescence images of perylene NCs measured by means of SNOM (JASCO, NFS-320, Japan).[49] From these data, one can obtain the fluorescence emission spectra of single perylene NCs with different crystal size as shown in Figure 5. There are the two main emission peaks: one is a strong and broad peak from the STE level at longer wavelength region, and the other is relatively weak and sharp peak from the free-exciton (FE) level. The STE emission peak positions were evidently blue-shifted with decreasing crystal size, while the crystal size did not almost affect the FE emission peak positions within experimental errors. These relations are summarized and plotted in Figure 6. The size dependence has been discussed in detail on the basis of a strong coupling model of exciton–

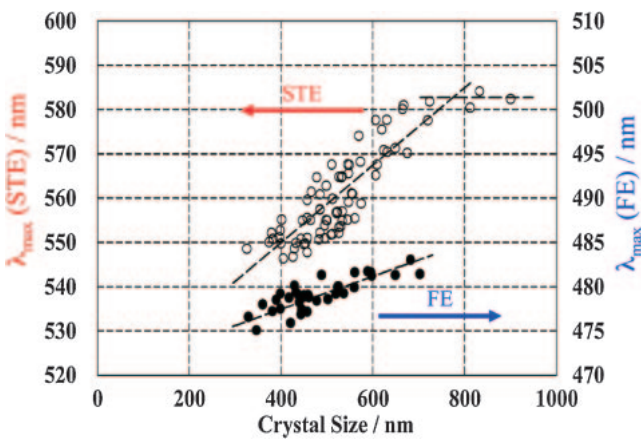

Figure 6. Plots of STE and FE emission peak positions vs. crystal size in a single perylene NC.

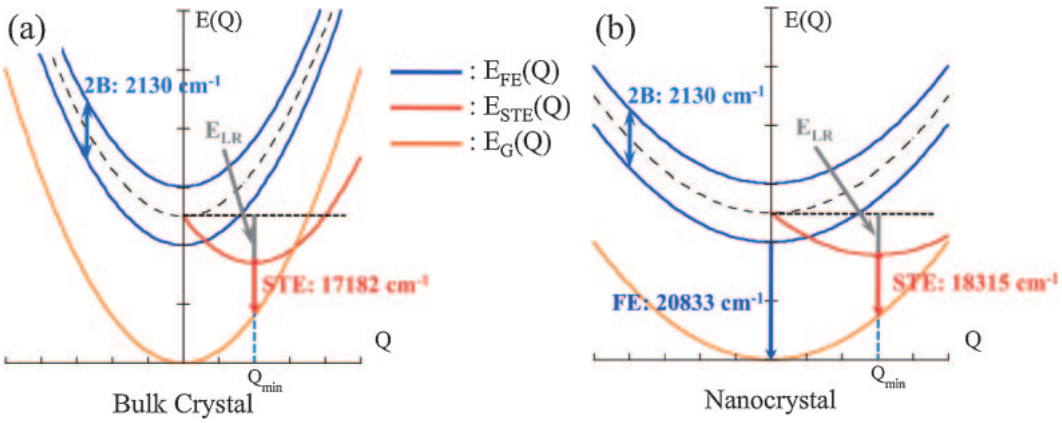

Figure 7. Strong coupling model of exciton–lattice interaction in the short range for molecule crystal, configuration coordinate model, in the cases of (a) bulk crystal and (b) NC.

lattice interaction in the short range for molecular crystal, the configuration coordinate model, as illustrated in Figure 7.[49]

The three adiabatic potential curves, i.e., ground state, FE, and STE levels, are represented schematically against generalized coordinate Q in a bulk crystal (Figure 7a) and NC (Figure 7b), respectively, in which 2B denotes the excitonic band. The curvature ω of three adiabatic potential curves is assumed to be all the same in the present case, and means an angular frequency of phonon in lattice vibration, which corresponds to the bulk modulus of lattice. The lattice relaxation energy E_{LR} is usually too high in bulk crystal, and only STE emission may be generated at Q_{min} represented by $(2E_{LR}/\omega)^{1/2}$. On the contrary, the following is speculated in the case of perylene NCs. Probably, it becomes difficult to reorientate and stabilize excited perylene molecules, i.e., Frenkel exciton, in perylene NC lattice so as to acquire sufficient E_{LR}, due to the thermal softening of organic NC lattice[23–25,49,50,52] induced by both enlargement of surface area and decreasing intermolecular interaction. Namely, the values of ω and E_{LR} are reduced, and Q_{min} simultaneously increases by assuming the decrement of $\delta(2E_{LR}) < \delta\omega$ as shown in Figure 7b. In other words, organic NC lattice can be regarded to be in general metastable, and the band gap energy at Q_{min} is increased, compared with bulk crystal. In addition, FE emission observed in a NC can be explained by the reduction of E_{LR}. That is to say, an exciton on the STE level could thermally go back to the FE level over the relatively lower energy barrier between FE and STE levels.

Size dependence of linear optical properties in organic NCs is of great importance for optical device application as well as nanoscience.

4. Core–Shell Type Hybridized Organic Nanocrystals

As mentioned in the Introduction, PDA is a typical one-dimensional π-conjugated polymer with large $\chi^{(3)}(\omega)$ and high optically fast response among organic NLO materials,[63–66] and PDA NCs exhibit the peculiar size dependence of linear optical properties, due to the thermally softened NC lattice.[23–25] The $\chi^{(3)}(\omega)$ value of PDA, however, is still low for NLO device application. On the other hand, LSP in noble metal NPs has been widely investigated for enhancement of optically electric field and fluorescence emission intensity,[16–18,97,98] so-called surface-enhanced Raman spectroscopy (SERS), and chemical- and biosensors applications. A coupling between exciton and LSP at the core–shell interface would provide a new hybrid electronic state and novel optical response for next-generation organic photonic materials and devices.[26–31] Thus, it is said that the important points are to establish a fabrication for core–shell type hybridized organic NCs in order to control core–shell interface structure and to further investigate mutual interaction at the core–shell interface,[32] which is still now poorly understood, compared with heterojunctions between semiconductor and metal.[33]

4.1 Polymer Core–Metal Shell Hybridized Nanocrystals. Hybridized organic NCs composed of PDA NCs core and Ag NPs shell, i.e., PDA core–Ag shell hybridized NCs, have been successfully fabricated by the following photocatalytic reduction method,[85] which exploits the absorption of vis light by the PDA core, because of excitonic absorption along the π-conjugation polymer backbone chain.[63] In this method, a given amount of $AgNO_3$ aq and NH_3 aq are first added into a PDA NCs dispersion liquid, which has been previously prepared by reprecipitation method, and then vis light should be irradiated for typically 30 min at 40 °C, using a Xenon lamp (USHIO, 500 W) equipped with attenuator and UV-cut filter ($\lambda > 420$ nm). NH_3 aq was added to form a diamminesilver complex $[Ag(NH_3)_2]^+$ and to control pH in the dispersion liquid. Actually, PDA core may act as a photocatalysis and substrate as discussed later.

Figure 8 shows the SEM and transmission electron microscopy (TEM) (JEOL, JFM-2000X, Japan) images of the resulting hybridized NCs.[85] A large number of bright white and black dots correspond to the deposited Ag NPs in SEM and TEM images, respectively. Thus, as a Ag shell, 5 to 15 nm Ag NPs were densely deposited only on the surface of PDA core. There were no isolated Ag NPs observed in either SEM or TEM images. The electron-diffraction (ED) pattern (the inset in TEM image) clearly exhibits Debye–Scherrer rings, i.e., ED from (111), (200), (220), and (311) planes in the fcc crystal lattice of bulk Ag (JCPDS: 4-783). In addition, powder XRD (Bruker, AXS, D8 Advance, USA) pattern (Figure 9) and EPMA (JEOL, JXA-8200, Japan) data (Figure 10) also demonstrated obviously that the metal NPs deposited on PDA core are not silver oxide but really Ag.

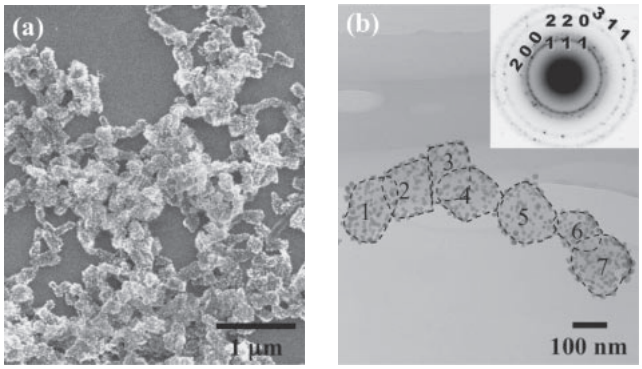

Figure 8. (a) SEM and (b) TEM images of PDA core–Ag shell hybridized NCs fabricated by photocatalytic reduction method. The inset in TEM image is the corresponding ED pattern.

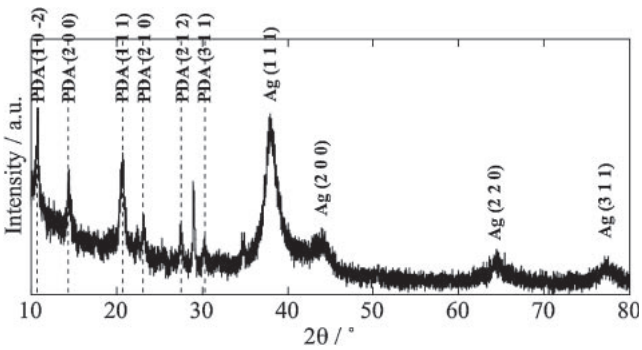

Figure 9. Powder XRD pattern of PDA core–Ag shell hybridized NCs.

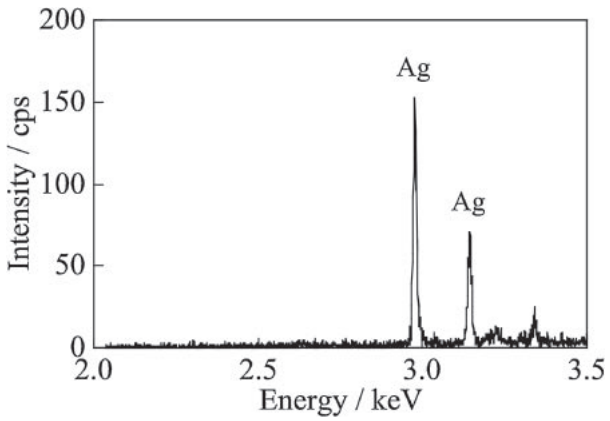

Figure 10. EPMA data of PDA core–Ag shell hybridized NCs.

Figure 11 displays photographs of the dispersion liquids of PDA NCs and PDA core–Ag shell hybridized NCs, and the corresponding extinction spectra are shown in Figure 12.[85] In the comparison with the LSP ($\lambda = 395$ nm) of bare Ag NPs with the same size (diameter = ca. 10 nm) as the Ag NPs deposited on PDA core,[97] the LSP in the hybridized organic NCs was obviously red-shifted to $\lambda = 448$ nm and the half-width was broadened. The red shift of LSP is mainly induced by the enlargement of dipole–dipole interaction with the decrease in average distance among the deposited Ag NPs,[98] as

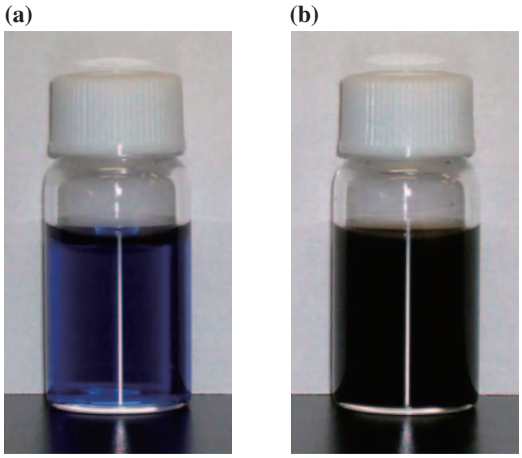

Figure 11. Photographs of (a) PDA NCs and (b) PDA core–Ag shell hybridized NCs dispersed in an aqueous dispersion medium.

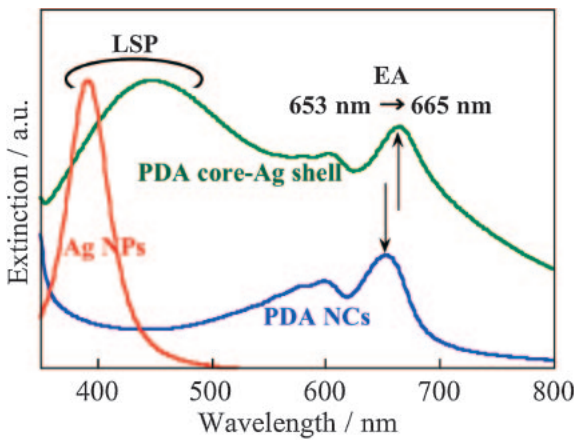

Figure 12. Extinction spectra of Ag NPs (diameter = ca. 10 nm), PDA NCs, and PDA core–Ag shell hybridized NCs.

photocatalytic reduction method may proceed. On the contrary, the broadening is not so clear and complicated. Perhaps, this is due to inhomogeneous distribution in size and the dephasing effect in Ag NPs grown and deposited on PDA core.[98–101] On the other hand, the EAP ($\lambda = 653$ nm)[63] was also red-shifted slightly, owing to changes of dielectric environment in the surrounding PDA core surface. In any case, these spectral changes in Figure 12 may support the formation of PDA core–Ag shell hybridized NCs as shown in Figures 8 to 10. The LSP spectrum in these hybridized organic NCs was tailed and overlapped on EAP. This suggests a certain coupled interaction between plasmon and exciton in the present case.[13,14,26–31]

The mechanism of photocatalytic reduction process is speculated in Figure 13.[85] Interestingly, Ag^+ (actually, $[Ag(NH_3)_2]^+$) from $AgNO_3$ was not reduced thoroughly by vis light irradiation in the absence of PDA NCs as a core or in the presence of solid-state unpolymerized DA monomer NCs that do not absorb vis light.[85] Namely, the present photocatalytic reduction process may occur specifically only on the surface of or in the coexistence of PDA core. The typical band structure of PDA is conduction band (CB) = −3.44 eV, valence

band (VB) = −5.77 eV, and the band gap = 2.33 eV,[102] which corresponds to $\lambda = 530$ nm in the vis light region and is different from EPA. On the other hand, the redox potential of $[Ag(NH_3)_2]^+$ is 0.373 V vs. SHE (= −4.873 eV),[85] which is located in the band gap between CB and VB for PDA. As demonstrated in Figure 13, the excited electrons from VB to CB of PDA core by absorbing vis light could specifically reduce $[Ag(NH_3)_2]^+$ to Ag^0 on the surface of PDA core. Subsequently, the nucleation and crystal growth of Ag^0 may further proceed, and then Ag NPs are deposited only on the surface of PDA core.

There are some advantages in surface-specific reduction of $[Ag(NH_3)_2]^+$ on PDA core in the present photocatalytic reduction method: (1) the electrostatic adsorption of $[Ag(NH_3)_2]^+$ on PDA core with ζ-potential (MALVERN, Zeta Sizer Nano Series, U.K.) = ca. −40 mV,[44] (2) the self-catalytic effect of already-deposited Ag NPs to further promote the reduction of $[Ag(NH_3)_2]^+$,[103] and (3) suppression of electron–hole recombination because of rapid carrier separation at the core–shell interface.

The pH of the dispersion liquid was changed roughly from 9 to 6 during this photocatalytic reduction process. This suggests that the hole generated in VB of vis light-irradiated PDA core could be quenched possibly by the oxidation of the surrounding water molecules in the dispersion liquid as expressed by the following oxidation process:

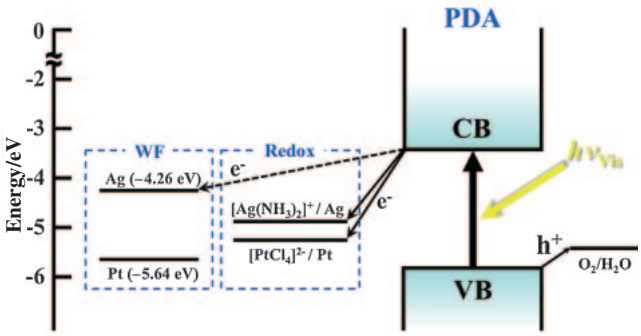

Figure 13. Proposed mechanism of photocatalytic reduction process. CB and VB of PDA, the redox potential of metal complex ions, and the WF of the corresponding metals are referred to the text.

$$2H_2O + 4h^+ \rightarrow O_2 + 4H^+ \quad (1)$$

In addition, the pH dependence of redox potential for water molecule is given by[104]

$$E_{redox}(H_2O)\ [\text{V vs. SHE}] = 1.23 - 0.059 \times \text{pH} \quad (2)$$

Namely, the reduction process does not take place under acidic conditions. It is difficult to scavenge holes in VB of PDA core by oxidizing water molecule, when pH is low.

4.2 Extension of Photocatalytic Reduction Method. The most important point is that the redox potential of metal complex ion should be intermediate between CB and VB for π-conjugated organic and polymer core, and the hole generated in VB should be quenched immediately through a suitable oxidation process of scavenger.[85] In other words, the present photocatalytic reduction process may proceed, independent of the size, shape, and morphology of organic core.[85] Some examples are summarized in Figure 14:[91] PDA core–Pt shell hybridized NCs, fibrous PDA core–Pt shell hybridized NCs, and poly(3-octylthiophene) (PAT)[33] core–Pt shell hybridized NCs. The deposited metal shells were identified evidently by measurement with the ED pattern from TEM images, powder XRD patterns, and EPMA data. The preparation process of these hybridized organic NCs is basically the same as that of previous PDA core–Ag shell hybridized NCs. Namely, $K_2[PtCl_4]$ was employed, instead of $AgNO_3$, to produce Pt shells. The redox potential of $[PtCl_4]^{2-}$ is 0.73 V vs. SHE (= −5.23 eV) and located well in the band gap of PDA core.[91] Fibrous PDA NCs were fabricated carefully by the conventional reprecipitation method,[23] when the temperature of water as a poor solvent was ca. 60 °C. PAT is also a π-conjugated polymer in semi-crystalline state,[105] and PAT NPs could be successfully fabricated as a core by reprecipitation method using THF as a good solvent. PAT has a shallow band structure (CB = −2.85 eV and VB = −5.25 eV)[106] rather than PDA, and so the hole should be quenched by oxidization of a small amount of added formaldehyde, E_{redox}(HCHO) = 0.197 V vs. SHE as follows.[104]

$$HCHO(aq) + 2H_2O + 4h^+ \rightarrow CO_3^{2-} + 6H^+ \quad (3)$$

One can see that Pt NPs are deposited more densely on PDA and PAT cores, and that the average size is too small and below 5 nm from TEM images in Figure 14, compared with the case

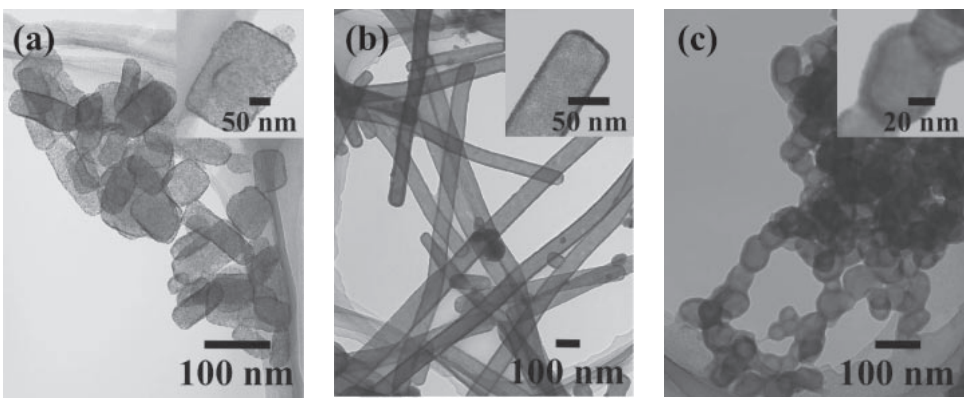

Figure 14. TEM images of (a) PDA core–Pt shell hybridized NCs, (b) fibrous PDA core–Pt shell hybridized NCs, and (c) PAT core–Pt shell hybridized NCs.

of Ag NPs as shown in Figure 8. This difference in average size and deposition density between Ag and Pt NPs could be reasonably explained on the basis of the relationship between redox potential of metal complex ion and work function (WF) of the deposited metal as displayed in Figure 13.[91] The WFs of Ag and Pt are, respectively, −4.26 and −5.64 eV.[91] Thus, the WF level is higher than the redox potential in the case of Ag. Hence, the excited electrons may usually transfer to the WF level, once Ag NPs are initially deposited on PDA core. As a result, already-deposited Ag NPs may further grow. On the other hand, the relation is reverse in the case of Pt, and the excited electrons may always move to the redox potential level. Thus, Pt complex may be mainly reduced only on the surface of PDA core, and then the average size decreases with high deposition density. Simply stated, the relative correlation between WF and redox potential may affect remarkably the morphology of the metal shell. Of course, the following experimental conditions should be optimized to produce well-defined core–shell type hybridized organic NCs:[85,91] added amount and concentration of metal complex salt, pH control, reaction temperature and time, stirring rate, and intensity and wavelength of vis light, except for the selected combination of π-conjugated polymer as a core and noble metal as a shell. Just recently, it was found that ultrasonic wave irradiation is much more effective than mechanical stirring.

4.3 Metal Nanoshell Structure by Post Chemical Reduction Treatment. Already-deposited Ag or Pt NPs on the surface of PDA or PAT core can be regarded as a new reduction starting point or a self-catalysis for alternative and subsequent reduction process and electroless plating.[91]

For example, it seems to be difficult to experimentally deposit Au NPs on PDA core, because the redox potential of $[AuCl_4]^-$ (=1.002 V vs. SHE) is very close to the redox potential of water given by eq 2 as well as VB for PDA. In addition, since $H[AuCl_4]$ may absorb vis light somewhat, $[AuCl_4]^-$ is reduced directly in the dispersion liquid as well as on PDA core. As a result, nondeposited Au NPs are also formed at the same time. The post chemical reduction treatment can be applied to overcome this problem. In fact, a given amount of $H[AuCl_4]$(aq) and ascorbic acid (reducing agent) were added an aqueous dispersion liquid of PDA core–Ag shell hybridized NCs, and then the mixture was stirred at room temperature for a given time. The reduction of $[AuCl_4]^-$ by the added ascorbic acid may start selectively on the surface of already-deposited Ag NPs on PDA core as self-catalysis. Figure 15 demonstrates the SEM image of Au(-Ag) NPs deposition on PDA core, i.e., PDA core–Au shell hybridized NCs, and this formation was supported experimentally by EPMA data (Figure 16a) and the corresponding extinction spectral changes (Figure 16b). The LSP peak of Ag NPs was reduced gradually, while the LSP peak from Au NPs appeared around at 560 nm. Both deposited Ag NP and Au NP domains formed inside the metal shell are much smaller than the wavelength in vis light, and the effective dielectric constant may correspond to Ag–Au alloy. That is to say, the LSP in Figure 16b may reflect the dielectric constant of Ag–Au alloy,[107,108] being not the simply additive extinction spectra from individual Ag NPs and Au NPs.[91] However, the powder XRD pattern has not been measured, because the fcc lattice constant of Au ($a = 0.408$ nm) is almost the same as that of Ag (fcc: $a = 0.409$ nm).[109]

In addition, the uses of $K_2[PtCl_4]$ and $Na_2[PdCl_4]$ have successfully led to Pt(-Ag) NPs and Pd(-Ag) NPs depositions on the surface of PDA core, respectively.[110–112] Ascorbic acid was also used as a reducing agent.

Figure 17 demonstrates the TEM image of Pt(-Pt) NPs deposition on PDA core, i.e., PDA core–Pt shell hybridized NCs having Pt nanoshell structure.[91] $K_2[PtCl_4]$(aq) and formaldehyde (reducing agent) were further added into PDA core–Pt

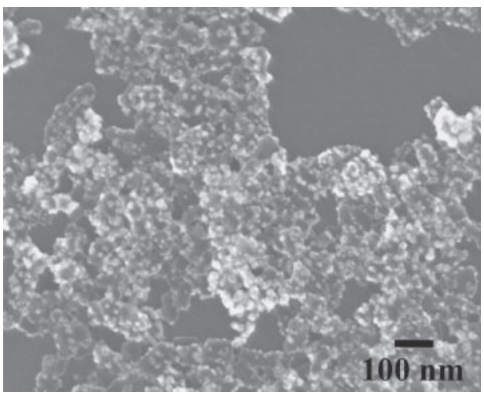

Figure 15. SEM image of Au(-Ag)-deposited PDA NCs.

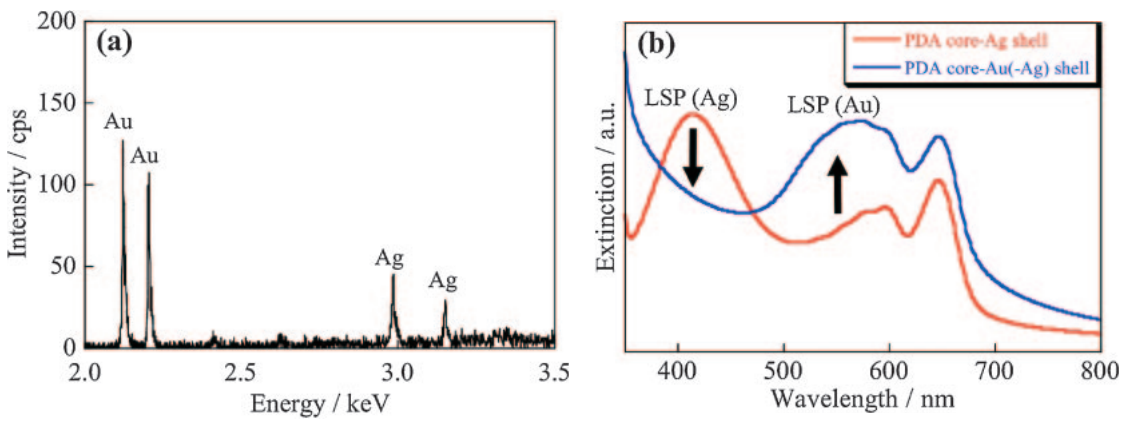

Figure 16. (a) EPMA data of PDA core–Au(-Ag) shell hybridized NCs, and (b) extinction spectral changes with the post chemical reduction treatment.

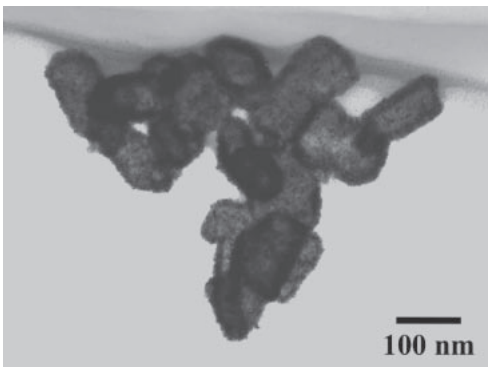

Figure 17. TEM image of Pt(-Pt)-deposited PDA NCs.

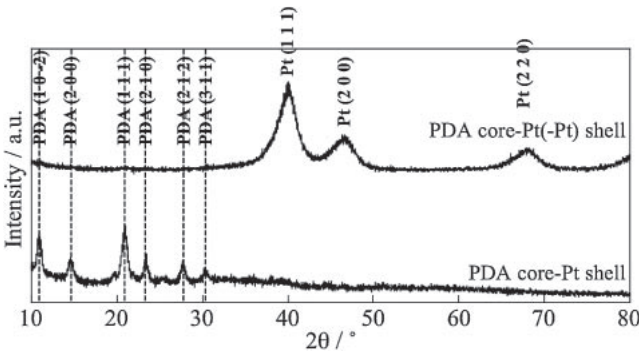

Figure 18. Powder XRD patterns of PDA core–Pt shell hybridized NCs and PDA core–Pt(-Pt) shell hybridized NCs.

shell hybridized NCs dispersion liquid in this case. One can control easily the thickness of Pt nanoshell by changing the amount of $K_2[PtCl_4]$ and formaldehyde. After the post chemical reduction treatment, the XRD peaks from PDA core disappeared and the broad (111) diffraction peak from Pt NPs grew up at the same time in the powder XRD patterns as shown in Figure 18,[109] which also supports the formation of thicker Pt nanoshell structure on PDA core. In addition, Pt(-Pt) NPs deposition on PAT core could be fabricated successfully by using $K_2[PtCl_4]$, poly(vinylpyrrolidone) as a dispersion stabilizer, and formic acid as a reducing agent.

4.4 Nonlinear Optical Properties. Neeves et al. have theoretically predicted the enhancement of NLO properties, $\chi^{(3)}(\omega)$ value, in the case of π-conjugated polymer core–metal shell hybridized NCs, due to enlargement of optically electric field induced by LSP.[113] For example, the values of $\chi^{(3)}(\omega)$ were, respectively, calculated to be 1×10^{-5} esu (shell: Au) and 2×10^{-4} esu (shell: Al) by reference to $\chi^{(3)}(\omega) = 1 \times 10^{-7}$ esu for only PDA core. So-called Z-scan method [Nd-YAG pulsed laser (EKSMA: PL2143A, 20ps, 5 Hz), OPG/OPA (EKSMA, SHG crystal: LBO (420 to 1800 nm), diamond pinhole ($d = 100\,\mu m$), Si-photodetector (Molelectron, J3S-10), LabView (National Instruments)] was employed to evaluate $\chi^{(3)}(\omega)$ value in the present PDA core–Ag shell hybridized NCs, and then the $\chi^{(3)}(\omega)$ value was confirmed for the first time to be enhanced by about two orders of magnitude ($\chi^{(3)}(\omega) \approx 10^{-6}$ to 10^{-5} esu).[114] Further detailed analyses, e.g., power dependence of incident laser light, wavelength dispersion corresponding to extinction spectrum, and scattering effect

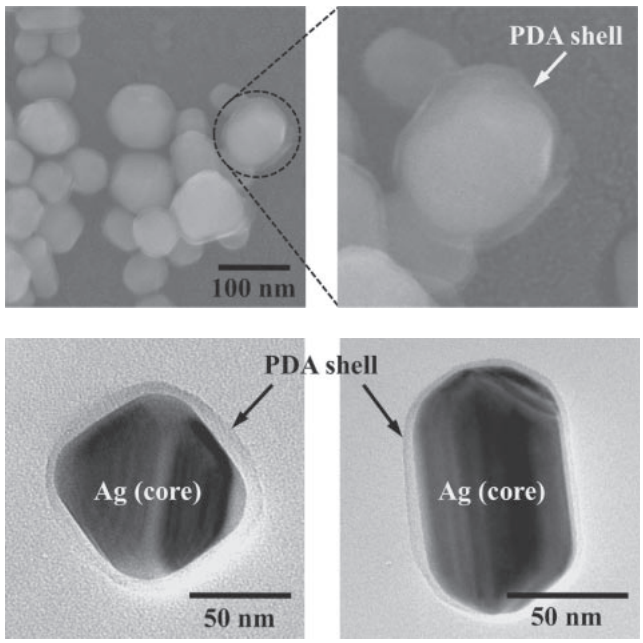

Figure 19. SEM (upper) and TEM (lower) images of Ag core–PDA shell hybridized NCs.

from thin film of PDA core–Ag shell hybridized NCs prepared by layer-by-layer process, are currently under investigation to determine $\chi^{(3)}(\omega)$ value very precisely.[114] In particular, it is important to prepare the thin film of hybridized organic NCs of optically high quality without scattering loss. The improved tapered cell method,[115,116] as described in Section **5**, as well as the previous layer-by-layer process[70–72] is now attempted for the purpose of bringing about a maximum performance in $\chi^{(3)}(\omega)$ value as well as highly accurate measurement.

4.5 Metal Core–Polymer Shell Hybridized Nanocrystals. This core–shell nanostructure is an inverse of that described in the previous Sections, and Ag core–PDA shell hybridized NCs could be also fabricated successfully by establishing the co-reprecipitation and microwave irradiation method.[77,82] An aqueous dispersion liquid of Ag NPs was employed as a poor medium, which was previously prepared by the reduction of $AgNO_3$ using trisodium citrate.[117] In fact, an acetone solution of DA monomer (commonly 5 mM and 200 μL) was injected into an aqueous dispersion liquid of Ag NPs, and subsequently the mixed dispersion liquid was quickly heated by microwave irradiation (2.45 GHz, 500 W, 40 s). After cooling to room temperature, UV-irradiation ($\lambda = 254$ nm) was performed for solid-state polymerization to convert DA to PDA.[94–96] Figure 19 indicates the SEM and TEM images of Ag core–PDA shell hybridized NCs. Ag core is coated with the very thin layer of PDA shell,[82] which suggests that Ag core may act as a nucleus to adsorb DA monomer and to form solid-state polymerizable DA shell by heat treatment during microwave irradiation process.

Figure 20 shows the peculiar extinction spectral changes during solid-state polymerization, when PDA with *N*-carbazolyl side chain was used as a shell.[77] Namely, the EPA grew at ca. 655 nm with UV-irradiation time, due to formation of π-conjugated PDA backbone, while the intensity of LSP from Ag core at around 395 nm was continuously reduced and

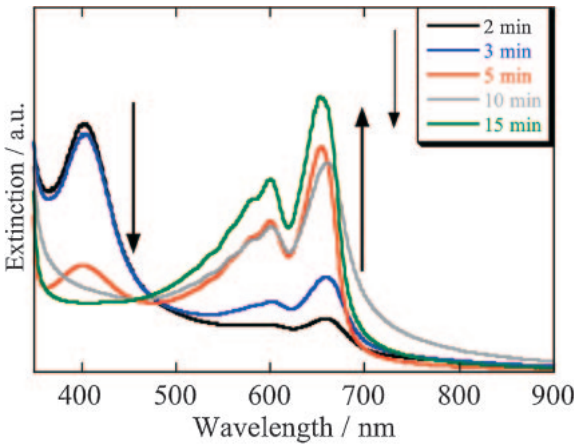

Figure 20. Extinction spectral changes during solid-state polymerization for Ag core–DA (having *N*-carbazolyl side chain) shell hybridized NCs.

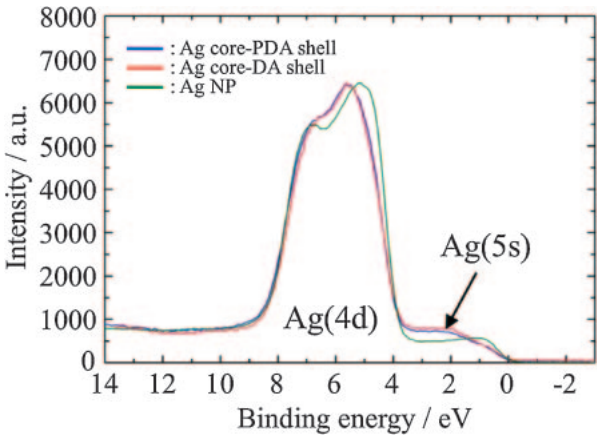

Figure 21. SR-XPS spectra of Ag core–PDA (having *N*-carbazolyl side chain) shell hybridized NCs.

disappeared at the same time without changing resonance frequency. The intensity of LSP is often damped with changing resonance frequency in some cases such as metal alloys and metal NPs in glass matrix.[118,119] Interestingly, no LSP damping was observed in the case of UV-irradiated mixture of Ag NPs and the same DA monomer NCs dispersion liquids, and the obtained extinction spectrum indicates the additives of both spectra from Ag NPs and PDA NCs.[77] Probably, the LSP damping is closely related to the EPA growth, due to specific electronic interaction at the core–shell interface in the present case.

For the purpose of revealing the damping mechanism of LSP, synchrotron radiation X-ray photoelectron spectroscopy (SR-XPS) and X-ray absorption near-edge structure (XANES) were measured at SPring-8 (BL15XU),[79,81] and this beam line is a revolver type (planar or helical) undulator X-ray source with Si double crystal monochromator (4.75 keV and $\delta E/E = 10^{-4}$), which is managed by the National Institute for Materials Science (NIMS, Japan). The XPS analyzer used is the modified one based on a ULVAC-PHI 10–360 model hemispherical analyzer. The binding energy was calibrated with not the Fermi edge but the corresponding C(1s) = 284.8 eV, and $L_3M_{4,5}M_{4,5}$ Auger intensity in L_3-absorption edge was monitored in XANES. There was scarcely a difference in XANES before and after solid-state polymerization, which was almost in agreement with that of bulk Ag, not with silver oxide. These data support speculation that physicochemical changes such as oxidation did not occur in Ag core during solid-state polymerization. In other words, Ag core is still metallic in the hybridized organic NCs. The XPS bands, Ag(5s) and Ag(4d), in Ag core–PDA shell (with *N*-carbazolyl side chain) hybridized NCs are shown in Figure 21.[79,81] Ag(5s) is often hybridized with Ag(4d) band even in bulk Ag state. Ag(5s) band exhibits a gentle slope at Fermi edge, and the intensity, corresponding to DOS, became higher in comparison with bulk Ag. In addition, Ag(4d) band was clearly shifted by about 0.4 eV to high binding energy region, and the band width became narrow. Probably, a different type hybrid band of Ag(5s) and Ag(4d) would be formed in the present hybridized organic NCs. The narrowing of Ag(4d) band strongly suggests that the electronic conductive domain inside Ag core is below ca. 5 nm,[120] which is actually less than the overall size of Ag core. This domain in Ag core may behave as a resistive boundary against collective oscillation and mean-free-path (MFP) of conduction free electrons in VB of Ag core that is the origin of LSP. On the other hand, the C(1s) band (284.8 eV) from PDA shell was incidental to the satellite peak (ca. 292 eV), owing to π–π^* transition in PDA,[121] and was distinctly broadened and tailed asymmetrically the high energy region. This fact suggests an electron-poor state in PDA shell.

These experimental results would make a possible to propose the following LSP damping mechanism.[79,81,120,122] PDA chains inside the shell may keep a locally and physicochemically strong contact and interaction like chemisorption and/or chemical band formation at some or many points on the surface of Ag core. The contact points at the core–shell interface can be regarded as a kind of anchors to disturb and depress the collective oscillation inside Ag core, which may lead to the dramatic reduction of MFP and then LSP intensity damping without changing resonance frequency.

5. Ordered Array Structure toward Optically Functional Materials

Next-generation organic devices in optoelectronics and photonics have some advantages over inorganic silicon devices:[9,10,12,30,32,123] various molecule designs and modifications for functional materials, high performance and response, easy fabrication process, low cost, and so on. On the other hand, it is in general difficult to maintain thermal stability and long material life, to continuously repeat device actions with highly reliability, and to standardize material products.

For organic optoelectronic and photonic device application by the use of organic NCs including hybridized organic NCs, one needs establish fabrication processes to fairly produce an ordered array structure on a substrate.[86,87,123] In other words, it would be necessary to well orientate and arrange organic NCs and to further integrate and assemble them selectively on a substrate so as to control input and output information signals by electronically and/or optically accessing organic devices.[123–126] However, there are mainly two problems to realize this.[92] One is that the shape of organic NCs is usually not

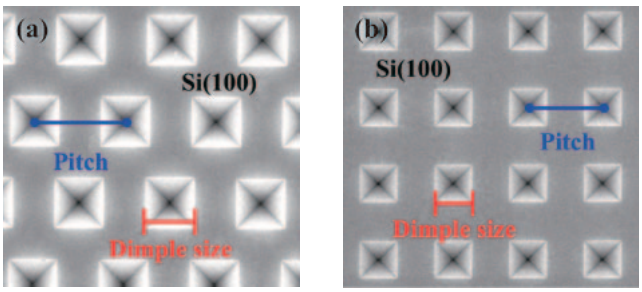

Figure 22. SEM images of (a) hexagonally and (b) tetragonally patterned Si(100) substrates prepared by EB-lithography and the subsequent anisotropic wet etching.

spherical but cubic or rectangular, and the other is commonly the size distribution. To overcome and dissolve these problems, our attention is now intensively focused on (A) encapsulation of organic NCs,[92] (B) the use of lithographically patterned substrate,[90] and (C) the employment of so-called tapered cell method.[115,116] Encapsulation may provide some merits: pseudo-monodisperse in size of organic NCs, spherical shape, and passivation effect for stable dispersion. On the other hand, a patterned substrate is very effective to selectively and precisely control the position and location for encapsulated organic NCs so as to assemble and integrate an ordered array structure.[127,128] So far, sedimentation method under gravity effect,[129] crystallization induced by capillary force,[130] and dewetting process[131] are well known to fabricate self-assembled micro- and nano-structure on a flat substrate for photonic device applications using polymer microspheres (or polymer colloidal particles) and colloidal silica particles.[123] However, these techniques cannot be unexpected to produce an ordered array structure for organic NCs. On the contrary, the present combination of above-mentioned techniques (A) to (C) would be definitively superior to the previous methods in the cases of organic NCs,[90,92] including polymer microspheres (or polymer colloidal particles) and colloidal silica particles.

Figure 22 shows typical patterned Si(100) substrates, which were prepared by electron beam (EB) lithography and subsequent anisotropic wet etching.[90] There exist regularly inverse square-pyramidal dimples with hexagonal or tetragonal symmetry, which is defined as the dimple size (L) and the pitch (P) between dimples. These patterned Si substrates used have an advantage of allowing encapsulated organic NCs to integrate with the present Si-based semiconductor devices. The set-up of tapered cell method is schematically illustrated in Figure 23,[115,116] where a cover glass was slightly tilted (ca. 1 to 2°) on a patterned Si substrate that has been previously surface-treated with piranha solution. For example, an aqueous dispersion liquid of polystyrene microspheres (PSMS) should be injected into the space between tilted cover glass and patterned substrate in the tapered cell under controlled conditions of PSMS dispersion concentration, temperature (ca. 20 °C), and humidity (ca. 40%). Consequently, PSMS would be trapped into the dimples by drawing back of the meniscus, and the residual PSMS not trapped by the dimples is completely dragged and swept with moving the meniscus. Thus, there is no PSMS on the terrace of the patterned substrate. This process could be basically repeated to further

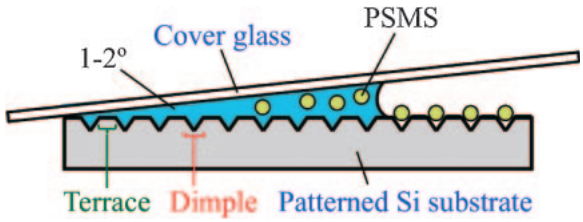

Figure 23. Schematic set-up of tapered cell method.

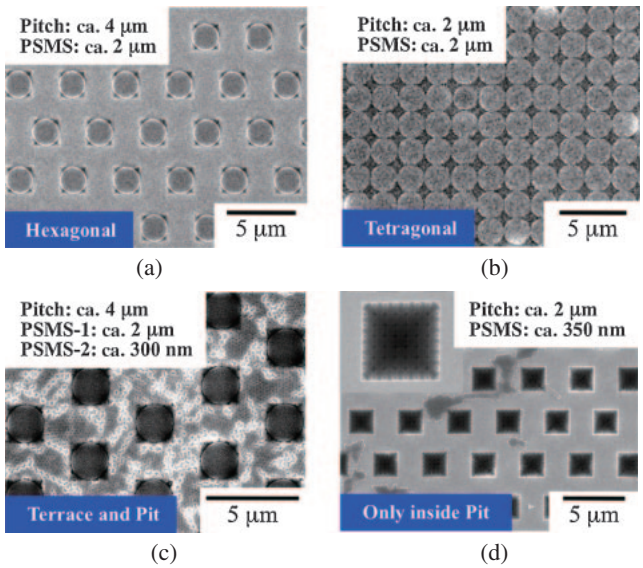

Figure 24. SEM images of some kinds of ordered PSMS array structure on the patterned substrate: (a) hexagonal array structure, (b) tetragonal array structure, (c) large ($D = 2\,\mu$m)- and small ($D = 300$ nm)-sized PSMS are, respectively, trapped into the dimples and only on the terrace of the patterned substrate, and (d) small-sized PSMS ($D = 300$ nm) are closely filled up only inside the dimples.

trap PSMSs on the first layer of ordered PSMS array structure as a template.[90,92]

5.1 Ordered Array Structure of PSMS. Ordered array structure could be designed conveniently by optimizing the parameters of L and P, pattern symmetry, and the diameter (D) of PSMS.[88–90,93] Figure 24 demonstrates some examples of ordered PSMS array structure on a patterned substrate.[90] Figures 24a and 24b indicate the hexagonal and tetragonal array structure of PSMS on the patterned substrate. Interestingly, Figure 24c shows that the large-sized PSMS ($D = 2\,\mu$m) are trapped into the dimples and the small-sized PSMS ($D = 300$ nm) are located only on the terrace of the patterned substrate by means of the repeated tapered cell method.[124,125] On the other hand, the small-sized PSMS ($D = 300$ nm) are closely filled up only inside the dimples as shown in Figure 24d.[124]

Figure 25 exhibits so-called Kagome structure[132] consisting of PSMS that is the second layer of ordered array structure by repeating the tapered cell method. Kagome structures made up by dielectric rods or wire networks are now theoretically investigated and there is much interest in the large flat photonic bands and magnetic properties, superior to honeycomb struc-

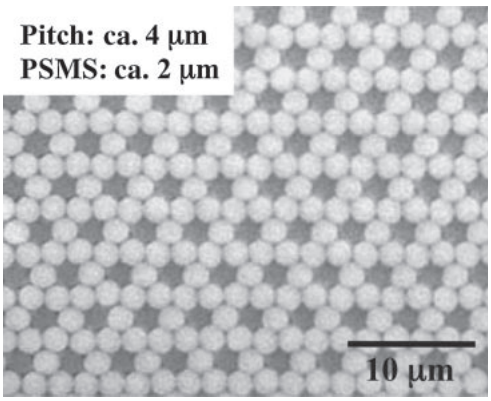

Figure 25. SEM image of Kagome structure of PSMS on hexagonally patterned substrate.

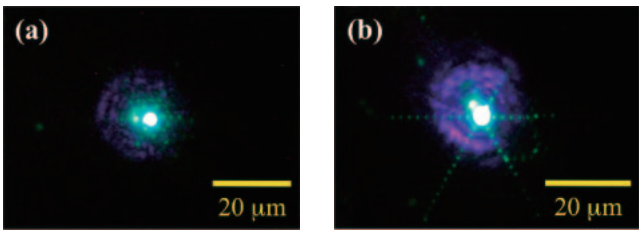

Figure 26. Far-field optical images of light propagation from fluorescent PSMS in (a) Kagome structure and (b) ordinary hexagonally close-packed PSMS structure on a flat substrate.

ture.[133–135] In addition, Kagome structure is said to exhibit a confinement effect of light propagation. Hence, the Kagome structure containing a small amount of the same-sized fluorescent PSMS could be successfully prepared again in order to confirm this. One can see experimentally the confinement of light propagation from fluorescent PSMS in Kagome structure (Figure 26a) by reference to ordinary hexagonally close-packed PSMS structure on a flat substrate as shown in Figure 26b.[136] In other words, a novel ordered array structure consisting of PSMS would contribute open new research fields of optical waveguide and optical wiring between CPUs or between semiconductor chips.[123,136]

It is also possible to repeat the tapered cell procedure, after the first-ordered array structure on the patterned substrate is rotated at 90°. One can obtain the ordered PSMS array structure with branching points, i.e., 90°-corner structure on tetragonally patterned substrate, as shown in the SEM image of Figure 27.[89] As already discussed in Figure 26, ordered PSMS array structure can be regarded as a coupled-resonator optical waveguide (CROW) to control and manipulate the light propagation path. The light propagation behavior from fluorescent PSMS at the branching point has been elaborately investigated by measurement with a handmade SNOM instrument mounted with a GaN-based laser diode ($\lambda = 406$ nm). The spot size was ca. 10 μm, and the propagated light was collected with a bent type of cantilevered optical fiber probe, i.e., far-field illumination and near-field collection mode. Figure 28 indicates the real light propagation spectrum (upper Figure),[89] in which Point-A and Point-B are the positions before and beyond the branching point, respectively. The

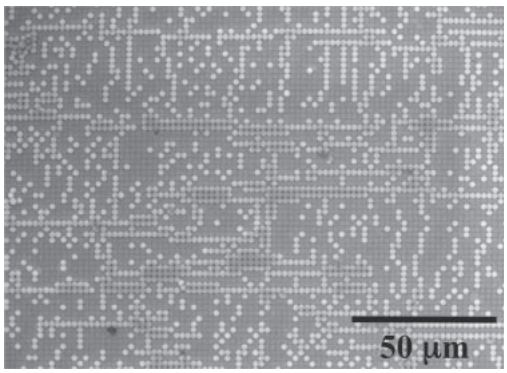

Figure 27. SEM image of ordered PSMS array structure with branching points, i.e., 90°-corner structure, on tetragonally patterned substrate.

scattering spectrum (lower Figure) from a single PSMS calculated using the Mie theory[137] is also displayed in Figure 28. Here, $TE_{n,l}$ and $TM_{n,l}$ denote the polarization type, i.e., transverse electric and transverse magnetic, and the subscripts n and l are an angular number and a radial quantum number, respectively. Interestingly, the intensity of $TE_{16,1}$ at Point-B is much lower (or approximately zero) than those of $TM_{15,1}$ and $TM_{16,1}$. This tendency is the same as the intensities of $TE_{15,1}$ and $TE_{17,1}$. The experimentally most important point is that the relative intensity of $TM_{16,1}$ at Point-A is completely different from that at Point-B, compared with the intensity of $TM_{15,1}$. Namely, it has become clearly apparent that $TM_{16,1}$ does not propagate through the branching point at a 90°-corner structure.[89] This behavior could be reproduced well by FDTD simulation.[89] In other words, this kind of ordered PSMS array structure would be expected to exhibit the possibility of multiplexer and/or demultiplexer.[93]

5.2 Ordered Array Structure of Encapsulated Semiconductor Nanoparticles. Encapsulated semiconductors such as CdS and ZnS NPs have been fabricated before encapsulating organic NCs. CdS and ZnS NPs were produced by so-called gel–sol method.[138] For example, a gelatin aqueous solution, which contained $Cd(OH)_2$, EDTA-2Na, ammonium acetate, NH_3 aq, and thioacetamide as a source of S^{2-}, was heated at 60 °C for about 10 h. After removing gelatin and by-products, the resulting CdS NPs were redispersed stably in an aqueous dispersion medium. On the other hand, ZnS NPs aqueous dispersion liquid was also prepared by the same procedure using $Zn(NO_3)_2$. Figure 29 shows the SEM images of CdS and ZnS NPs, which are spherical and almost monodisperse in size. ZnS NPs have smooth surface, compared to the case of CdS NPs.

The obtained CdS and ZnS NPs were further encapsulated by means of seed-emulsion polymerization process.[92] Namely, CdS and ZnS NPs dispersion liquids were refluxed at 80 °C under nitrogen atmosphere by adding styrene (St) monomer, divinylbenzene (DVB) as a crosslink agent, and potassium peroxodisulfide (KPS) initiator, followed by purification using centrifugation instrument, and then redispersed in an aqueous dispersion medium. As a result, CdS and ZnS NPs were successfully encapsulated with transparent and weakly cross-linked polystyrene (PS) shell, i.e., PS-encapsulated CdS and ZnS microparticles (MPs), as shown in Figure 30.[92] The white

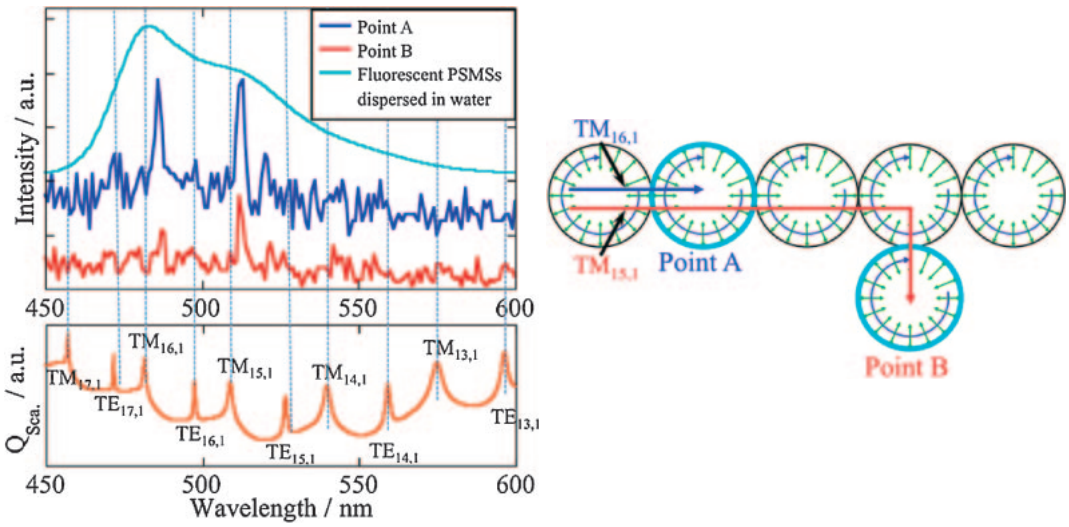

Figure 28. Light propagation spectra before (Point A) and beyond (Point B) the branching point, (upper Figure) and the corresponding scattering spectrum from a single PSMS calculated using the Mie theory (lower Figure).

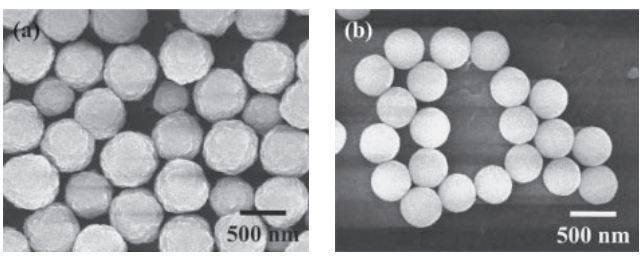

Figure 29. SEM images of (a) CdS and (b) ZnS NPs.

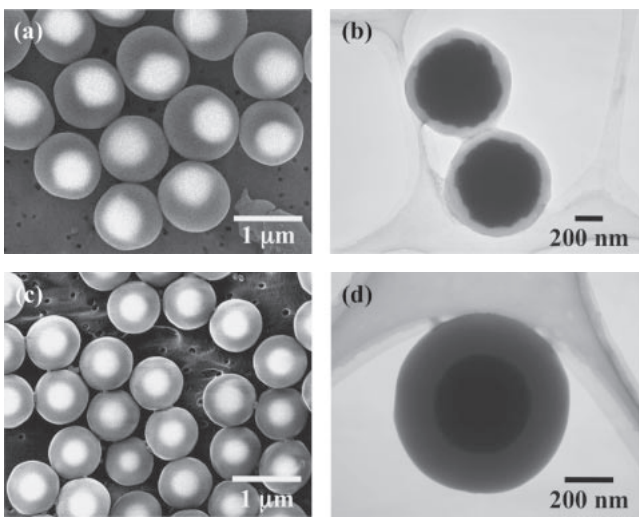

Figure 30. (a, c) SEM and (b, d) TEM images of PS-encapsulated (a, b) CdS and (c, d) ZnS MPs.

area in the SEM image and the black part in the TEM image correspond to CdS and ZnS NPs, respectively. The thickness of PS shell could be controlled conveniently by repeating a series of seed-emulsion polymerization process. A small amount of added surfactant sodium dodecyl sulfate (SDS) was applicable for encapsulation of ZnS NPs, but not so in the case of CdS NPs. That is, the inside morphology of the resulting encapsulated MPs would be influenced remarkably by the difference in

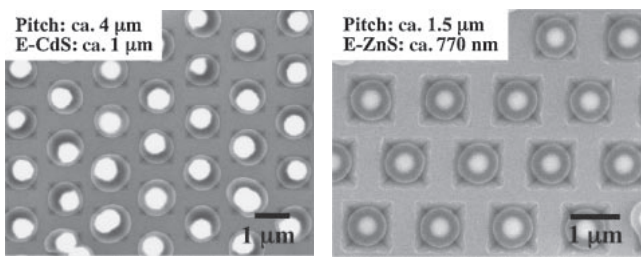

(a) (b)

Figure 31. SEM images of ordered array structure for PS-encapsulated (a) CdS and (b) ZnS MPs.

affinity among St, the formed PS, SDS, and semiconductor NPs. Actually, ZnS NP was approximately centered inside the encapsulated MP, whereas CdS NP was out of the central part as shown in Figure 30.

Both PS-encapsulated CdS and ZnS MPs are clearly spherical, and the size is almost uniform. Hence, one can prepare easily the ordered array structures of these PS-encapsulated CdS and ZnS MPs on hexagonally patterned substrate using the same tapered cell method as shown in Figure 31.[92] Probably, the rate of stepping back of the meniscus should be further optimized so as to obtain a large area of ordered array structure, compared with PSMS case, because CdS or ZnS NP has a higher specific gravity than PSMS. In addition, PS-encapsulated semiconductor MPs indicated higher ζ-potentials, which are -65 and -54 mV with CdS and ZnS, respectively, than the bare semiconductor NPs (ca. -23 mV), owing to the sulfo-residual fragments originating from decomposed KPS on the surface of PS shell.

5.3 Ordered Array Structure of Encapsulated Polydiacetylene Nanocrystals. PDA NCs were also encapsulated successfully by basically using the same procedure. PDA NCs dispersion liquids previously prepared by reprecipitation method[23] were condensed and then used without dialysis treatment. The conductivity of the PDA NCs condensed dispersion liquid was over 1000 μS. Soap-free seed-emulsion copolymerization was performed under the following condi-

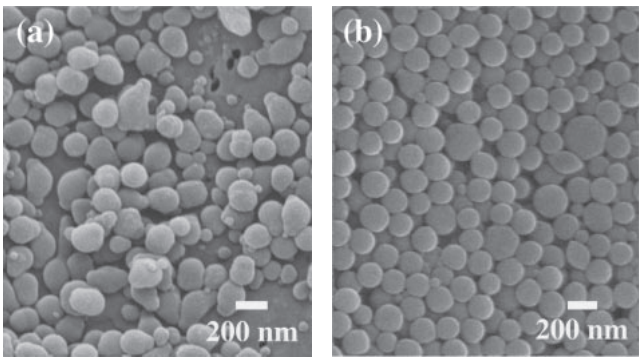

Figure 32. SEM images of PDA NCs encapsulated with (a) only PS and (b) poly(St-*co*-HSt).

tions.[92,139] St monomer, DVB, KPS, and hydrophilic styrene derivative monomer (HSt: 1-(4-vinylphenyl)ethane-1,2-diol) were added into PDA NCs dispersion liquids. SDS was not added in the present soap-free case. The mixture of the dispersion liquids was refluxed at 80 °C and 1000 rpm under nitrogen atmosphere at the molar ratio of St:HSt = 99:1. Copolymerization and encapsulation processes were monitored with ^{1}H NMR, IR, and the extinction spectrum, and the thickness of poly(St-*co*-HSt) shell could be controlled by repeatedly adding the mixed monomer of St and HSt under the same molar ratio.[92]

Figure 32 demonstrates the SEM images of PDA NCs encapsulated with only PS or with poly(St-*co*-HSt), respectively.[92] Evidently, PS-encapsulated PDA NCs was not spherical but irregular, and a large number of isolated PS NPs that do not contain PDA NCs were observed in the SEM image. In some cases of soap-free seed-emulsion polymerization, the dialysis treatment should be carried out for several days,[140] because high ionic strength would unexpectedly induce undesirable aggregation and segregation of seeds. However, interestingly, the present copolymerization of St and HSt may proceed successfully without dialysis treatment, and the encapsulated PDA NCs with poly(St-*co*-HSt) shell are almost spherical and uniform (ca. 95 nm) in size. In addition, the ζ-potential became higher (−66 mV), because of the above-mentioned same reason in the previous Section. The TEM image (Figure 33) obviously shows that rectangular PDA NCs was fully encapsulated and covered with spherical poly(St-*co*-HSt) shell, and the EAP from PDA NCs was observed at ca. 650 nm in the extinction spectrum of poly(St-*co*-HSt)-encapsulated PDA NCs.

The following two schemes of encapsulation mechanisms are now speculated:[92] (1) At the initial stage of copolymerization, St-*co*-HSt oligomers are first produced in a bulk aqueous medium, which have a higher affinity to PDA NCs than only St oligomers. As the copolymerization further proceeds, poly(St-*co*-HSt) may easily adsorb on the surface of PDA NCs and form a nucleus for polymer shell, due to the lowering of solubility in the water phase, and then encapsulation may take place completely at the surrounding of PDA NCs. On the other hand, (2) St fine droplets including HSt are assumed to exist near PDA NCs dispersed in aqueous dispersion medium. St fine droplets may be stabilized thermodynamically by the surface activity of hydrophilic HSt, and copolymerization starts on the surface of St fine droplets in the presence of PDA NCs. In both schemes, HSt is likely to be a kind of surfactant and may enhance the affinity and dispersion stability to finely form poly(St-*co*-HSt) shell. Probably, actual encapsulation may occur through the intermediate path between the above-mentioned (1) and (2) schemes.[92]

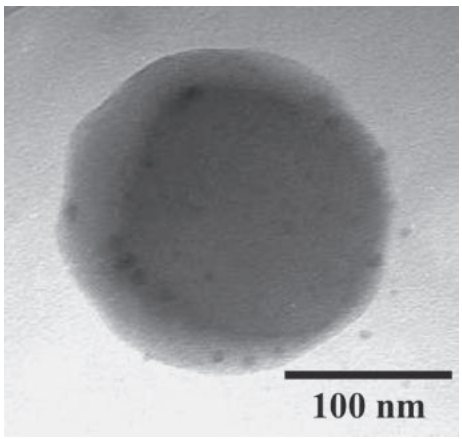

Figure 33. TEM image of poly(St-*co*-HSt)-encapsulated PDA NCs.

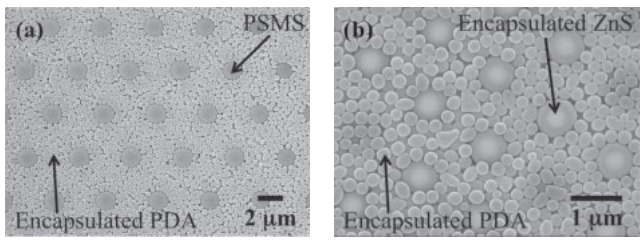

Figure 34. SEM images of the heterogeneously ordered array structure formed on the hexagonal patterned substrate: (a) PSMS in the dimple and poly(St-*co*-HSt)-encapsulated PDA NCs on the terrace, and (b) PS-encapsulated ZnS MPs in the dimple and poly(St-*co*-HSt)-encapsulated PDA NCs on the terrace.

In principle, it would be possible to arrange and produce ordered array structure of poly(St-*co*-HSt)-encapsulated PDA NCs on a patterned substrate, because of the almost spherical shape of poly(St-*co*-HSt)-encapsulated PDA NCs.[92] Figure 34 displays the SEM images of the heterogeneously ordered array structure formed on the hexagonal patterned substrate by using the repeated tapered cell method.[92] PSMS is inside the dimple and poly(St-*co*-HSt)-encapsulated PDA NCs are on the terrace in Figure 34a. On the other hand, PS-encapsulated ZnS MPs are trapped in the dimple and poly(St-*co*-HSt)-encapsulated PDA NCs exist on the terrace in Figure 34b. Heterogeneously ordered array structure composed of PSMS, encapsulated MPs and/or NCs having different optoelectronic and/or photonic properties will open a new path toward integrated device application such as functional photonic crystals and superlattice structure.

6. Concluding Remarks for Future Scope

The author has summarized and discussed the preparation techniques, structure analysis, and optical properties of organic NCs and the corresponding core–shell type hybridized organic

NCs. It has become feasible to perform mass-production process of organic NCs based on reprecipitation method, and SNOM measurements have revealed semiquantitatively the size dependence of linear optical properties for organic NCs, which is different from so-called quantum confinement effect in SQD. In addition, the present photocatalytic reduction method and the post chemical reduction treatment have been established to fabricate many kinds of core–shell type hybridized organic NCs and NPs. It was suggested for the first time that NLO properties would be enhanced in PDA core–Ag shell hybridized NCs, due to enlargement of optically electric fields induced by LSP from metal shells.[113] Further detailed analysis of obtained $\chi^{(3)}(\omega)$ value is now under investigation. It is also expected that this photocatalytic reduction method is applicable to create a nanoplating and meta-materials[141] in the near future.

On the other hand, some various kinds of ordered array structures have been successfully demonstrated on an EB-lithographically patterned substrate by introducing encapsulation process and the tapered cell method. First, Kagome structure consisting of PSMS prepared by the repeated tapered cell method has revealed the confinement effect of light propagation. Moreover, CdS and ZnS NPs were encapsulated conveniently with PS shell. The resulting PS-encapsulated semiconductor MPs were spherical and almost uniform in size, and it became possible to arrange ordered array structures on a patterned substrate. Rectangular PDA NCs were also encapsulated successfully with poly(St-*co*-HSt) shell. In particular, heterogeneously ordered array structure composed of PSMS, encapsulated semiconductor MPs, and encapsulated PDA NCs with the different type of optoelectronic and photonic properties is of great importance toward novel optoelectronic and photonic device application.[92]

Organic NCs, hybridized organic NCs, and the corresponding encapsulated organic NCs, including encapsulated semiconductor MPs and PSMS, can be regarded as promising building blocks in bottom-up processes. On the other hand, a patterned substrate is prepared by a typical top-down process. It is beyond question that these new building blocks are key materials,[142] and that the combination of bottom-up and top-down processes are of much interest and will be further advanced possibly toward next-generation organic and polymer devices for optoelectronics, nonlinear optics, and photonics in the near future,[143–145] e.g., flexible organic TFT, organic EL, organic photovoltaic, printed RF-ID, sensors, memory, e-paper, and so on. These organic and polymer device application would appear to be also useful and effective considerably to reduce resource, energy, and environmental problems on a global scale.

The author is greatly indebted to the following many collaborators for their kind scientific support and valuable discussion in order to extensively drive forward the present research projects: Emeritus Prof. H. Nakanishi (Tohoku Univ., Japan), Associate Prof. H. Kasai (IMRAM, Tohoku Univ., Japan), Assistant Prof. T. Onodera (IMRAM, Tohoku Univ., Japan), Prof. S. Okada (Graduate School of Sci. and Eng., Yamagata Univ., Japan), Assistant Prof. A. Masuhara (Graduate School of Sci. and Eng., Yamagata Univ., Japan), Emeritus Prof. H. Masuhara (Osaka Univ., Japan), Prof. T. Asahi (Graduate School of Sci. and Eng., Ehime Univ., Japan), Prof. T. Miyashita (IMRAM, Tohoku Univ., Japan), Prof. N. Nemoto (Faculty of Eng., Nihon Univ., Japan), Dr. T. Sekiguchi (National Institute for Materials Science (NIMS), Japan), Dr. S. Tanuma (NIMS, Japan), Dr. H. Yoshikawa (NIMS and SPring-8, Japan), Dr. Y. Wakayama (NIMS, Japan), Dr. T. Mitsui (NIMS, Japan), Dr. K. Miyazawa (NIMS, Japan), Dr. H. Matsuda (National Institute of Advanced Industrial Science and Technology (AIST), Japan), Dr. K. Yase (AIST, Japan), Dr. T. Fukuda (AIST, Japan), Dr. S. Shimada (AIST, Japan), the late Dr. T. Kimura (AIST, Japan), Emeritus Prof. O. Ito (Tohoku Univ., Japan), Emeritus Prof. K. Arai (Tohoku Univ., Japan), the late Prof. S. K. Tripathy (Univ. Massachusetts Lowell, USA), Prof. B. S. Wherrett (Herriot-Watt Univ., U.K.), Prof. Z.-F. Liu (Peking Univ., China), and all graduate school students in the laboratory.

References

1 X. Peng, M. C. Schlamp, A. V. Kadavanich, A. P. Alivisatos, *J. Am. Chem. Soc.* **1997**, *119*, 7019.
2 M. Valden, X. Lai, D. W. Goodman, *Science* **1998**, *281*, 1647.
3 X. Peng, L. Manna, W. Yang, J. Wickham, E. Scher, A. Kadavanich, A. P. Alivisatos, *Nature* **2000**, *404*, 59.
4 Y. Lu, Y. Yang, A. Sellinger, M. Lu, J. Huang, H. Fan, R. Haddad, G. Lopez, A. R. Burns, D. Y. Sasaki, J. Shelnutt, C. J. Brinker, *Nature* **2001**, *410*, 913.
5 L. M. Liz-Marzán, *Langmuir* **2006**, *22*, 32, and references cited therein.
6 For example: *Polymer Nanocomposites*, ed. by Y.-W. Mai, Z.-Z. Yu, Woodhead Publisher, Cambridge, **2006**.
7 B. Kraeutler, A. J. Bard, *J. Am. Chem. Soc.* **1978**, *100*, 4317.
8 A. Sellinger, P. M. Weiss, A. Nguyen, Y. Lu, R. A. Assink, W. Gong, C. J. Brinker, *Nature* **1998**, *394*, 256.
9 S. J. Oldenburg, R. D. Averitt, S. L. Westcott, N. J. Halas, *Chem. Phys. Lett.* **1998**, *288*, 243.
10 F. Caruso, *Adv. Mater.* **2001**, *13*, 11.
11 K. G. Thomas, P. V. Kamat, *Acc. Chem. Res.* **2003**, *36*, 888.
12 E. Prodan, C. Radloff, N. J. Halas, P. Nordlander, *Science* **2003**, *302*, 419.
13 G. P. Wiederrecht, G. A. Wurtz, J. Hranisavljevic, *Nano Lett.* **2004**, *4*, 2121.
14 G. A. Wurtz, P. R. Evans, W. Hendren, R. Atkinson, W. Dickson, R. J. Pollard, A. V. Zayats, W. Harrison, C. Bower, *Nano Lett.* **2007**, *7*, 1297.
15 W. Ni, Z. Yang, H. Chen, L. Li, J. Wang, *J. Am. Chem. Soc.* **2008**, *130*, 6692.
16 R. Jin, Y. Cao, C. A. Mirkin, K. L. Kelly, G. C. Schatz, J. G. Zheng, *Science* **2001**, *294*, 1901.
17 C. J. Murphy, N. R. Jana, *Adv. Mater.* **2002**, *14*, 80.
18 C. Loo, A. Lowery, N. Halas, J. West, R. Drezek, *Nano Lett.* **2005**, *5*, 709.
19 M. Bruchez, Jr., M. Moronne, P. Gin, S. Weiss, A. P. Alivisatos, *Science* **1998**, *281*, 2013.
20 R. F. Service, *Science* **2000**, *290*, 1526.
21 M. Nomura, N. Kumagai, S. Iwamoto, Y. Ota, Y. Arakawa, *Nat. Phys.* **2010**, *6*, 279.
22 F. X. Redi, K.-S. Cho, C. B. Murray, S. O'Brien, *Nature* **2003**, *423*, 968.

23 H. Oikawa, H. Kasai, H. Nakanishi, *Fabrication of Organic Microcrystals and Their Optical Properties* in *Anisotropic Organic Materials: Approaches to Polar Order (ACS Symposium Series 798)*, ed. by R. Glaser, P. Kaszynski, ACS, Washington, **2001**, Chap. 11, p. 158. doi:10.1021/bk-2001-0798.ch011; H. Oikawa, H. Kasai, H. Nakanishi, *Some Applications of Organic Microcrystals* in *Anisotropic Organic Materials: Approaches to Polar Order (ACS Symposium Series 798)*, ed. by R. Glaser, P. Kaszynski, ACS, Washington, **2001**, Chap. 12, p. 169. doi:10.1021/bk-2001-0798.ch012

24 H. Nakanishi, H. Oikawa, *Reprecipitation Method for Organic Nanocrystals* in *Single Organic Nanoparticles (Nano-Science and Technology)*, ed. by H. Masuhara, H. Nakanishi, K. Sasaki, Springer, Berlin, **2003**, Chap. 2, p. 17; H. Oikawa, H. Nakanishi, *Optical Properties of Polymer Nanocrystals* in *Single Organic Nanoparticles (NanoScience and Technology)*, ed. by H. Masuhara, H. Nakanishi, K. Sasaki, Springer, Berlin, **2003**, Chap. 14, p. 169; H. Oikawa, H. Nakanishi, *Particle-Based Optical Devices* in *Single Organic Nanoparticles (NanoScience and Technology)*, ed. by H. Masuhara, H. Nakanishi, K. Sasaki, Springer, Berlin, **2003**, Chap. 29, p. 382.

25 H. Oikawa, A. Masuhara, H. Kasai, T. Mitsui, T. Sekiguchi, H. Nakanishi, *Organic and Polymer Nanocrystals: Their Optical Properties and Function* in *Nanophotonics: Integrating Photochemistry, Optics and Nano/Bio Materials Studies*, ed. by H. Masuhara, S. Kawata, Elsevier, Amsterdam, **2004**, Chap. 13, p. 205.

26 A. Yoshida, Y. Yonezawa, N. Kometani, *Langmuir* **2009**, *25*, 6683.

27 Y. Sugawara, T. A. Kelf, J. J. Baumberg, *Phys. Rev. Lett.* **2006**, *97*, 266808.

28 C. Bonnand, J. Bellessa, J.-C. Plénet, *J. Non-Cryst. Solids* **2006**, *352*, 1683.

29 J. Bellessa, C. Bonnand, J. C. Plénet, J. Mugnier, *Phys. Rev. Lett.* **2004**, *93*, 036404.

30 N. T. Fofang, T.-H. Park, O. Neumann, N. A. Mirin, P. Nordlander, N. J. Halas, *Nano Lett.* **2008**, *8*, 3481.

31 J. Hranisavljevic, N. M. Dimitrijevic, G. A. Wurtz, G. P. Wiederrecht, *J. Am. Chem. Soc.* **2002**, *124*, 4536.

32 H. Oikawa, T. Onodera, A. Masuhara, H. Kasai, H. Nakanishi, *Adv. Polym. Sci.* **2010**, in press.

33 H. Ishii, K. Seki, *Energy Level Alignment at Organic–Metal Interfaces* in *Conjugated Polymer and Molecular Interfaces: Science and Technology for Photonic and Optoelectronic Applications*, ed. by W. R. Salaneck, K. Seki, A. Kahn, J.-J. Pireaux, Marcel Dekker Inc., New York, **2002**, Chap. 10, p. 293.

34 H. Kasai, H. S. Nalwa, H. Oikawa, S. Okada, H. Matsuda, N. Minami, A. Kakuta, K. Ono, A. Mukoh, H. Nakanishi, *Jpn. J. Appl. Phys.* **1992**, *31*, L1132.

35 H. Kamatani, H. Kasai, S. Okada, H. Matsuda, H. Oikawa, N. Minami, A. Kakuta, K. Ono, A. Mukoh, H. Nakanishi, *Mol. Cryst. Liq. Cryst.* **1994**, *252*, 233.

36 H. Katagi, H. Kasai, S. Okada, H. Oikawa, K. Komatsu, H. Matsuda, Z. Liu, H. Nakanishi, *Jpn. J. Appl. Phys.* **1996**, *35*, L1364.

37 H. Kasai, H. Kamatani, S. Okada, H. Oikawa, H. Matsuda, H. Nakanishi, *Jpn. J. Appl. Phys.* **1996**, *35*, L221.

38 H. Katagi, H. Kasai, S. Okada, H. Oikawa, H. Matsuda, H. Nakanishi, *J. Macromol. Sci., Part A: Pure Appl. Chem.* **1997**, *34*, 2013.

39 H. Matsuda, S. Yamada, E. van Keuren, H. Katagi, H. Kasai, S. Okada, H. Oikawa, H. Nakanishi, E. C. Smith, A. K. Kar, B. S. Wherrett, *Proc. SPIE* **1997**, *2998*, 241.

40 H. Kasai, Y. Yoshikawa, T. Seko, S. Okada, H. Oikawa, H. Matsuda, A. Watanabe, O. Ito, H. Toyotama, H. Nakanishi, *Mol. Cryst. Liq. Cryst.* **1997**, *294*, 173.

41 M. Fujitsuka, H. Kasai, A. Masuhara, S. Okada, H. Oikawa, H. Nakanishi, A. Watanabe, O. Ito, *Chem. Lett.* **1997**, 1211.

42 H. Kasai, H. Oikawa, S. Okada, H. Nakanishi, *Bull. Chem. Soc. Jpn.* **1998**, *71*, 2597.

43 H. Oikawa, T. Oshikiri, H. Kasai, S. Okada, S. K. Tripathy, H. Nakanishi, *Polym. Adv. Technol.* **2000**, *11*, 783.

44 T. Onodera, T. Oshikiri, H. Katagi, H. Kasai, S. Okada, H. Oikawa, M. Terauchi, M. Tanaka, H. Nakanishi, *J. Cryst. Growth* **2001**, *229*, 586.

45 R. G. Alargova, S. Deguchi, K. Tsujii, *J. Am. Chem. Soc.* **2001**, *123*, 10460.

46 T. Onodera, H. Kasai, S. Okada, H. Oikawa, K. Mizuno, M. Fujitsuka, O. Ito, H. Nakanishi, *Opt. Mater.* **2003**, *21*, 595.

47 B.-K. An, S.-K. Kwon, S.-D. Jung, S. Y. Park, *J. Am. Chem. Soc.* **2002**, *124*, 14410.

48 D. Xiao, L. Xi, W. Yang, H. Fu, Z. Shuai, Y. Fang, J. Yao, *J. Am. Chem. Soc.* **2003**, *125*, 6740.

49 H. Oikawa, T. Mitsui, T. Onodera, H. Kasai, H. Nakanishi, T. Sekiguchi, *Jpn. J. Appl. Phys.* **2003**, *42*, L111.

50 V. V. Volkov, T. Asahi, H. Masuhara, A. Masuhara, H. Kasai, H. Oikawa, H. Nakanishi, *J. Phys. Chem. B* **2004**, *108*, 7674.

51 Y. Kaneko, S. Shimada, T. Fukuda, T. Kimura, H. Yokoi, H. Matsuda, T. Onodera, H. Kasai, S. Okada, H. Oikawa, H. Nakanishi, *Adv. Mater.* **2005**, *17*, 160.

52 T. Asahi, T. Sugiyama, H. Masuhara, *Acc. Chem. Res.* **2008**, *41*, 1790, and references cited therein.

53 H. Nakanishi, H. Kasai, *Polydiacetylene Microcrystals for Third-Order Nonlinear Optics* in *Photonic and Optoelectronic Polymers (ACS Symposium Series 672)*, ed. by S. A. Jenekhe, K. J. Wynne, ACS, Washington, **1997**, Chap. 13, p. 183. doi:10.1021/bk-1997-0672.ch013

54 Y. Komai, H. Kasai, H. Hirakoso, Y. Hakuta, S. Okada, H. Oikawa, T. Adschiri, H. Inomata, K. Arai, H. Nakanishi, *Mol. Cryst. Liq. Cryst.* **1998**, *322*, 167.

55 Y. Komai, H. Kasai, H. Hirakoso, Y. Hakuta, H. Katagi, S. Okada, H. Oikawa, T. Adschiri, H. Inomata, K. Arai, H. Nakanishi, *Jpn. J. Appl. Phys.* **1999**, *38*, L81.

56 K. Baba, H. Kasai, S. Okada, H. Oikawa, H. Nakanishi, *Jpn. J. Appl. Phys.* **2000**, *39*, L1256.

57 K. Baba, H. Kasai, S. Okada, H. Nakanishi, H. Oikawa, *Mol. Cryst. Liq. Cryst.* **2006**, *445*, 161.

58 K. Ujiiye-Ishii, K. Baba, Z. Wei, H. Kasai, H. Nakanishi, S. Okada, H. Oikawa, *Mol. Cryst. Liq. Cryst.* **2006**, *445*, 177.

59 K. Baba, H. Kasai, A. Masuhara, S. Okada, H. Oikawa, H. Nakanishi, *Jpn. J. Appl. Phys.* **2007**, *46*, 7558.

60 K. Baba, H. Kasai, Y. Shinohara, S. Okada, H. Oikawa, H. Matsuda, H. Nakanishi, *Jpn. J. Appl. Phys.* **2008**, *47*, 3769.

61 K. Ujiiye-Ishii, E. Kwon, H. Kasai, H. Nakanishi, H. Oikawa, *Cryst. Growth Des.* **2008**, *8*, 369.

62 N. Tagawa, A. Masuhara, H. Kasai, H. Nakanishi, H. Oikawa, *Cryst. Growth Des.* **2010**, *10*, 2857.

63 G. Wegner, H. Bässler, H. Sixl, V. Enkelmann, *Polydiacetylene* in *Advances in Polymer Science*, ed. by H.-J. Cantow, Springer-Verlag, Berlin, **1984**, Vol. 63.

64 N. Bloembergen, *Nonlinear Optics*, World Science, Singapore, **1996**.

65 *Organic Nanophotonics*, ed. by F. Charra, V. M.

Agranovich, F. Kajzar, Kluwer Academic Publisher, London, **2003**.

66 P. N. Prasad, *Nanophotonics*, Willey-Interscience, Hoboken, **2004**.

67 H.-R. Chung, E. Kwon, H. Oikawa, H. Kasai, H. Nakanishi, *J. Cryst. Growth* **2006**, *294*, 459.

68 T. Tachikawa, H.-R. Chung, A. Masuhara, H. Kasai, H. Oikawa, H. Nakanishi, M. Fujitsuka, T. Majima, *J. Am. Chem. Soc.* **2006**, *128*, 15944.

69 S. Takahashi, H. Miura, H. Kasai, S. Okada, H. Oikawa, H. Nakanishi, *J. Am. Chem. Soc.* **2002**, *124*, 10944.

70 S. K. Tripathy, H. Katagi, H. Kasai, S. Balasubramanian, H. Oshikiri, J. Kumar, H. Oikawa, S. Okada, H. Nakanishi, *Jpn. J. Appl. Phys.* **1998**, *37*, L343.

71 J.-A. He, K. Yang, J. Kumar, S. K. Tripathy, L. A. Samuelson, T. Oshikiri, H. Katagi, H. Kasai, S. Okada, H. Oikawa, H. Nakanishi, *J. Phys. Chem. B* **1999**, *103*, 11050.

72 K. Yang, J.-A. He, J. Kumar, L. A. Samuelson, T. Oshikiri, H. Katagi, H. Kasai, S. Okada, H. Oikawa, H. Nakanishi, S. K. Tripathy, *J. Opt. Soc. Am. B* **2005**, *22*, 623.

73 S. Fujita, H. Kasai, S. Okada, H. Oikawa, T. Fukuda, H. Matsuda, S. K. Tripathy, H. Nakanishi, *Jpn. J. Appl. Phys.* **1999**, *38*, L659.

74 H. Oikawa, S. Fujita, H. Kasai, S. Okada, S. K. Tripathy, H. Nakanishi, *Colloids Surf., A* **2000**, *169*, 251.

75 S. Okazoe, S. Fujita, H. Kasai, S. Okada, H. Oikawa, H. Nakanishi, *Mol. Cryst. Liq. Cryst.* **2001**, *367*, 11.

76 H. Katagi, H. Kasai, S. Okada, H. Oikawa, H. Matsuda, H. Nakanishi, *Polym. Adv. Technol.* **2000**, *11*, 778.

77 A. Masuhara, H. Kasai, S. Okada, H. Oikawa, M. Terauchi, M. Tanaka, H. Nakanishi, *Jpn. J. Appl. Phys.* **2001**, *40*, L1129.

78 A. Masuhara, S. Ohhashi, H. Kasai, S. Okada, H. Oikawa, H. Nakanishi, *J. Nonlinear Opt. Phys. Mater.* **2004**, *13*, 587.

79 H. Oikawa, A. M. Vlaicu, M. Kimura, H. Yoshikawa, S. Tanuma, A. Masuhara, H. Kasai, H. Nakanishi, *Nonlinear Opt., Quantum Opt.* **2005**, *34*, 275.

80 A. Matsumoto, T. Ishikawa, T. Odani, H. Oikawa, S. Okada, H. Nakanishi, *Macromol. Chem. Phys.* **2006**, *207*, 361.

81 H. Yoshikawa, A. M. Vlaicu, M. Kimura, A. Masuhara, S. Tanuma, H. Nakanishi, H. Oikawa, *e-J. Surf. Sci. Nanotechnol.* **2009**, *7*, 711.

82 T. Yokoyama, A. Masuhara, T. Onodera, H. Kasai, H. Oikawa, *Synth. Met.* **2009**, *159*, 897.

83 T. Onodera, H. Oikawa, H. Kasai, H. Nakanishi, T. Sekiguchi, *Mater. Res. Soc. Symp. Proc.* **2004**, *846*, 257.

84 T. Onodera, Z. Tan, A. Masuhara, H. Oikawa, H. Kasai, H. Nakanishi, T. Sekiguchi, *Jpn. J. Appl. Phys.* **2006**, *45*, 379.

85 T. Onodera, H. Oikawa, A. Masuhara, H. Kasai, T. Sekiguchi, H. Nakanishi, *Jpn. J. Appl. Phys.* **2007**, *46*, L336.

86 Y. Wakayama, T. Mitsui, T. Onodera, H. Oikawa, H. Nakanishi, *Chem. Phys. Lett.* **2006**, *417*, 503.

87 Y. Wakayama, T. Mitsui, T. Onodera, H. Oikawa, H. Nakanishi, *e-J. Surf. Sci. Nanotechnol.* **2006**, *4*, 69.

88 T. Mitsui, Y. Wakayama, T. Onodera, Y. Takaya, H. Oikawa, *Nano Lett.* **2008**, *8*, 853.

89 T. Mitsui, Y. Wakayama, T. Onodera, Y. Takaya, H. Oikawa, *Opt. Lett.* **2008**, *33*, 1189.

90 T. Onodera, Y. Takaya, T. Mitsui, Y. Wakayama, H. Oikawa, *Jpn. J. Appl. Phys.* **2008**, *47*, 1404.

91 T. Onodera, J. Ujita, D. Ishikawa, A. Masuhara, H. Kasai, H. Oikawa, *ECS Trans.* **2009**, *16*, 1.

92 T. Onodera, M. Nakamura, Y. Takaya, A. Masuhara, Y. Wakayama, N. Nemoto, H. Nakanishi, H. Oikawa, *J. Phys. Chem. C* **2009**, *113*, 11647.

93 T. Mitsui, Y. Wakayama, T. Onodera, T. Hayashi, N. Ikeda, Y. Sugimoto, T. Takamasu, H. Oikawa, *Adv. Mater.* **2010**, *22*, 3022.

94 K. C. Yee, R. R. Chance, *J. Polym. Sci., Polym. Phys. Ed.* **1978**, *16*, 431.

95 V. Enkelmann, R. Leyrer, G. Schleier, G. Wegner, *J. Mater. Sci.* **1980**, *15*, 168.

96 V. Enkelmann, G. Wenz, M. A. Müller, M. Schmidt, G. Wegner, *Mol. Cryst. Liq. Cryst.* **1984**, *105*, 11.

97 For example: M. Kerker, *J. Colloid Interface Sci.* **1985**, *105*, 297.

98 S. L. Westcott, S. J. Oldenburg, T. R. Lee, N. J. Halas, *Chem. Phys. Lett.* **1999**, *300*, 651.

99 K. E. Peceros, X. Xu, S. R. Bulcock, M. B. Cortie, *J. Phys. Chem. B* **2005**, *109*, 21516.

100 M. P. Pileni, A. Taleb, C. Petit, *J. Dispersion Sci. Technol.* **1998**, *19*, 185, and references cited therein.

101 K. Kuriyama, H. Kikuchi, Y. Oishi, T. Kajiyama, *Langmuir* **1995**, *11*, 3536.

102 W. Spannring, H. Bässler, *Chem. Phys. Lett.* **1981**, *84*, 54.

103 K. R. Brown, M. J. Natan, *Langmuir* **1998**, *14*, 726.

104 J. P. Hoare, *Oxygen* in *Standard Potentials in Aqueous Solution*, ed. by A. J. Bard, R. Parsons, J. Jordan, Marcel Dekker, New York, **1985**.

105 N. Kurokawa, H. Yoshikawa, N. Hirota, K. Hyodo, H. Masuhara, *ChemPhysChem* **2004**, *5*, 1609.

106 E. Kymakis, I. Alexandrou, G. A. J. Amaratunga, *J. Appl. Phys.* **2003**, *93*, 1764.

107 S. Link, Z. L. Wang, M. A. El-Sayed, *J. Phys. Chem. B* **1999**, *103*, 3529.

108 J. H. Hodak, A. Henglein, M. Giersig, G. V. Hartland, *J. Phys. Chem. B* **2000**, *104*, 11708.

109 H. P. Klug, L. E. Alexander, *X-ray Diffraction Procedures: For Polycrystalline and Amorphous Materials*, Wiley, New York, **1974**, p. 687.

110 K. Patel, S. Kapoor, D. P. Dave, T. Mukherjee, *J. Chem. Sci.* **2005**, *117*, 311.

111 H. N. Vasan, C. N. R. Rao, *J. Mater. Chem.* **1995**, *5*, 1755.

112 K. Torigoe, Y. Nakajima, K. Esumi, *J. Phys. Chem.* **1993**, *97*, 8304.

113 A. E. Neeves, M. H. Birnboim, *J. Opt. Soc. Am. B* **1989**, *6*, 787.

114 T. Onodera, J. Ujita, D. Ishikawa, K. Takahashi, A. Masuhara, H. Kasai, H. Nakanishi, H. Oikawa, manuscript in preparation.

115 T. Yamasaki, T. Tsutsui, *Jpn. J. Appl. Phys.* **1999**, *38*, 5916.

116 Y. Yin, Y. Lu, B. Gates, Y. Xia, *J. Am. Chem. Soc.* **2001**, *123*, 8718.

117 B. Vlckova, P. Matejka, J. Simonova, K. Cermakova, P. Pancoska, V. Baumruk, *J. Phys. Chem.* **1993**, *97*, 9719; A. Pyatenko, M. Yamaguchi, M. Suzuki, *J. Phys. Chem. B* **2005**, *109*, 21608.

118 U. Kreibig, M. Gartz, A. Hilger, *Ber. Bunsen-Ges. Phys. Chem* **1997**, *101*, 1593.

119 K. Hirakawa, N. Toshima, *Chem. Lett.* **2003**, *32*, 78.

120 P. Mulvaney, *Langmuir* **1996**, *12*, 788.

121 A. Dilks, *X-ray Photoelectron Spectroscopy for the Investigation of Polymeric Materials* in *Electron Spectroscopy: Theory, Techniques and Application*, ed. by C. R. Brundle, A. D. Baker, Academic Press, London, **1981**, Vol. 4, p. 277.

122 S. G. Louie, J. R. Chelikowsky, M. L. Cohen, *Phys. Rev. B* **1977**, *15*, 2154.
123 *Colloids and Colloid Assemblies: Synthesis, Modification, Organization and Utilization of Colloid Particles*, ed. by F. Caruso, Wiley-VCH Verlag GmbH & KGaA, Weinheim, **2004**.
124 A. van Blaaderen, R. Ruel, P. Wiltzius, *Nature* **1997**, *385*, 321.
125 G. A. Ozin, S. M. Yang, *Adv. Funct. Mater.* **2001**, *11*, 95.
126 E. Botzung-Appert, J. Zaccaro, C. Gourgon, Y. Usson, P. L. Baldeck, A. Ibanez, *J. Cryst. Growth* **2005**, *283*, 444.
127 S. Matsuo, T. Fujine, K. Fukuda, S. Juodkazis, H. Misawa, *Appl. Phys. Lett.* **2003**, *82*, 4283.
128 Y. Yin, Z.-Y. Li, Y. Xia, *Langmuir* **2003**, *19*, 622.
129 D. H. Everett, *Basic Principles of Colloid Science*, Royal Society of Chemistry, London, **1988**.
130 N. Denkov, O. Velev, P. Kralchevski, I. Ivanov, H. Yoshimura, K. Nagayama, *Langmuir* **1992**, *8*, 3183.
131 O. Karthaus, S. Mikami, Y. Hashimoto, *J. Colloid Interface Sci.* **2006**, *301*, 703.
132 J. B. Nielsen, T. Søndergaard, S. E. Barkou, A. Bjarklev, J. Broeng, M. B. Nielsen, *Electron. Lett.* **1999**, *35*, 1736.
133 K. Shiraishi, H. Tamura, H. Takayanagi, *Appl. Phys. Lett.* **2001**, *78*, 3702.
134 H. Takeda, T. Takashima, K. Yoshino, *J. Phys.: Condens. Matter* **2004**, *16*, 6317.
135 R. Gajić, R. Meisels, F. Kuchar, K. Hingerl, *Phys. Rev. B* **2006**, *73*, 165310.
136 S. Grego, T. W. Jarvis, B. R. Stoner, J. S. Lewis, *Langmuir* **2005**, *21*, 4971.
137 H. C. van de Hulst, *Light Scattering by Small Particles*, Dover Pub. Inc., New York, **1981**.
138 T. Sugimoto, G. E. Dirige, A. Muramatsu, *J. Colloid Interface Sci.* **1996**, *180*, 305; T. Sugimoto, G. E. Dirige, A. Muramatsu, *J. Colloid Interface Sci.* **1996**, *182*, 444.
139 D. Zou, V. Derlich, K. Gandhi, M. Park, L. Sun, D. Kriz, Y. D. Lee, G. Kim, J. Aklonis, R. Salovey, *J. Polym. Sci., Part A: Polym. Chem.* **1990**, *28*, 1909.
140 Z. Wei, K. Ujiiye-Ishii, A. Masuhara, H. Kasai, S. Okada, H. Matsune, T. Asahi, H. Masuhara, H. Nakanishi, *J. Nanosci. Nanotechnol.* **2005**, *5*, 937.
141 A. Ishikawa, T. Tanaka, *Opt. Commun.* **2006**, *258*, 300.
142 D. Horn, J. Rieger, *Angew. Chem., Int. Ed.* **2001**, *40*, 4330.
143 A. L. Briseno, S. C. B. Mannsfeld, M. M. Ling, S. H. Liu, R. J. Tseng, C. Reese, M. E. Roberts, Y. Yang, F. Wudl, Z. N. Bao, *Nature* **2006**, *444*, 913.
144 M. J. Currie, J. K. Mapel, T. D. Heidel, S. Goffri, M. A. Baldo, *Science* **2008**, *321*, 226.
145 K. Y. Cheng, R. Anthony, U. R. Kortshagen, R. J. Holmes, *Nano Lett.* **2010**, *10*, 1154.

Hidetoshi Oikawa completed his M.Sc. work at Tohoku University in 1980, and was a Research Associate at the Chemical Research Institute of Non-Aqueous Solutions, Tohoku University. He holds a Doctoral Degree in chemistry from Tohoku University in 1987, and joined the group of Prof. H. Nakanishi as a Research Associate at Institute for the Chemical Reaction Science (ICRS), Tohoku University in 1991. From 1992 to 1993, he worked as a Visiting Research Fellow at the Max-Planck-Institut für Polymerforschung (MPIP) (Laboratory of Solid Chemistry: Prof. G. Wegner) and BASF-AG (Division of Solid-State Physics: the late Dr. D. Horn), Germany. Returning to Tohoku University, he joined again the Nakanishi Laboratory, and was promoted to Associate Professor in 1994. From 2002 to 2005, he was a Senior Researcher at the National Institute for Materials Science (NIMS) in Tsukuba, Japan, and was promoted to Full Professor at the Institute of Multidisciplinary Research for Advanced Materials (IMRAM), Tohoku University in 2006. Throughout his career, he has engaged in fabrication, characterization, hybridization, and assembled nanostructure in π-conjugated organic and polymer nanocrystals toward optoelectronic and photonic devices applications.